

---

# DCR: Counterfactual Attractor Guidance for Rare Compositional Generation

---

Taewon Kang<sup>1</sup>, Matthias Zwicker<sup>1</sup>

<sup>1</sup>University of Maryland at College Park, United States  
taewon@umd.edu, zwicker@umd.edu

## Abstract

Diffusion models generate realistic visual content, yet often fail to produce *rare but plausible compositions*. When prompted with combinations that are valid but underrepresented in training data—such as *a snowy beach* or *a rainbow at night*—the generation process frequently collapses toward more common alternatives. We identify this failure mode as *default completion bias*, where denoising trajectories are implicitly attracted toward high-frequency semantic configurations. Existing guidance mechanisms do not explicitly model this competing tendency and therefore struggle to prevent such collapse. We introduce **Default Completion Repulsion (DCR)**, a training-free framework that explicitly models and suppresses default completion behavior. DCR constructs a *counterfactual attractor* by relaxing the rare compositional factor while preserving surrounding semantics, inducing an alternative denoising trajectory reflecting the model’s preferred completion. We define the discrepancy between target and attractor trajectories as a *counterfactual drift*, and propose a projection-based repulsion mechanism that removes guidance components aligned with this drift direction. This suppresses undesired frequent completions while preserving other semantic components. DCR operates entirely within the standard diffusion sampling process without retraining or architectural modification. Experiments on rare compositional prompts show that DCR improves compositional fidelity while maintaining visual quality. Our analysis further shows that the framework exposes and counteracts intrinsic model biases, offering a new perspective on controllable generation beyond explicit constraint enforcement.

## 1 Introduction

Diffusion models have achieved remarkable success in image and video generation. Despite this progress, they exhibit a persistent limitation: they struggle to generate *rare but plausible compositions*. When given prompts that combine semantically valid elements that rarely co-occur in training data—such as *a penguin in a desert*, *a snowy beach*, or *a rainbow at night*—the generated outputs often deviate from the intended description and instead reflect more common visual patterns. This phenomenon can be understood as a form of *compositional collapse*. During denoising, the model is implicitly biased toward high-frequency semantic configurations, causing the trajectory to drift away from the specified rare composition and toward a more likely alternative. Importantly, this failure mode does not arise from ambiguous prompts or missing constraints, but from the model’s intrinsic preference for statistically dominant patterns. Existing approaches to controllable generation primarily focus on *reinforcing the target signal*, for example by increasing guidance strength, introducing additional conditioning inputs, or modifying attention mechanisms. However, these methods do not explicitly account for the presence of competing completion tendencies within the model. As a result, even strong conditioning may fail to prevent collapse when the desired composition lies in a low-density region of the learned distribution.

In this work, we propose a fundamentally different perspective. Instead of strengthening the target signal, we explicitly identify and suppress the model’s *default completion tendency*. Our key insight is that this tendency can be revealed through a *counterfactual attractor* constructed by relaxing the original prompt. By weakening the rare compositional factor while preserving the surrounding semantic context, the transformed prompt induces an alternative denoising trajectory that reflects the model’s preferred completion. Building on this idea, we introduce **Default Completion Repulsion**

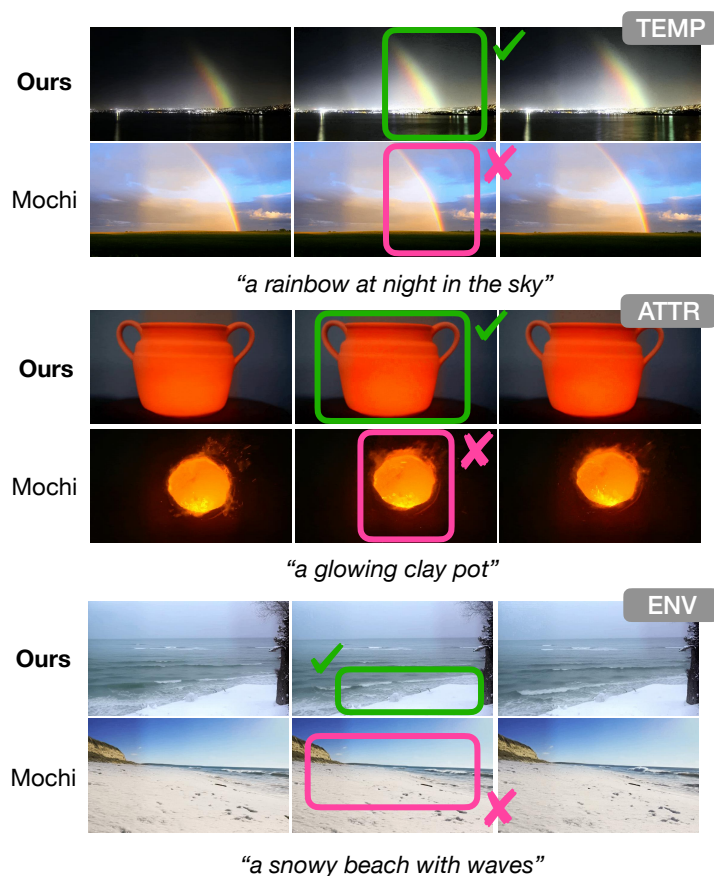


Figure 1: **Default completion bias in video diffusion models.** We compare our method (DCR) against Mochi on three representative rare compositional prompts spanning Temporal Misalignment (TEMP), Attribute Rebinding (ATTR), and Environment Recomposition (ENV). Baseline models collapse toward statistically dominant completions—generating a daytime rainbow instead of a nocturnal one, a glowing sphere instead of a glowing clay pot, and a snow-free beach instead of a snowy one. DCR explicitly models and suppresses this default completion tendency via counterfactual attractor guidance, faithfully realizing both compositional factors in each case. Extended comparisons across all eight compositional categories and additional baselines are provided in Section 4.3. **(DCR)**, a training-free framework that integrates seamlessly into the diffusion sampling process. At each denoising step, we compute both the target-guided update and the attractor-guided update, and define their difference as a *counterfactual drift*. We then apply a projection-based repulsion mechanism that removes the component of the update aligned with this drift direction. This prevents the denoising trajectory from collapsing toward frequent alternatives while preserving other semantic components. A key property of our approach is that the attractor trajectory is not constrained to be collinear with the standard guidance direction. This allows the method to capture genuinely distinct completion tendencies rather than merely rescaling the guidance strength, distinguishing it from prior guidance-based techniques. We evaluate our method on a benchmark of rare compositional prompts spanning object-scene, attribute-scene, and lighting-condition combinations. Our results show that DCR significantly improves compositional fidelity compared to standard classifier-free guidance and other baselines, while maintaining high visual quality. Further analysis demonstrates that our method effectively exposes and counteracts intrinsic model biases.

In summary, our contributions are as follows:

- We identify *compositional collapse* as a key failure mode in diffusion models for rare compositional generation.
- We propose a *counterfactual attractor* formulation that explicitly models the model’s default completion tendency via prompt relaxation.
- We introduce a projection-based repulsion mechanism that suppresses collapse during denoising.
- We demonstrate strong improvements in compositional fidelity, providing a new perspective on controllable generation beyond target-only guidance.

## 2 Related Work

### 2.1 Guidance Mechanisms for Diffusion Models

Classifier-free guidance (CFG) [18] is the dominant mechanism for conditioning diffusion models on text prompts. Several variants address its limitations, including dynamic thresholding [31], interval-based scheduling [8], and training-free modifications such as FreeU [33], Universal Guidance [3],

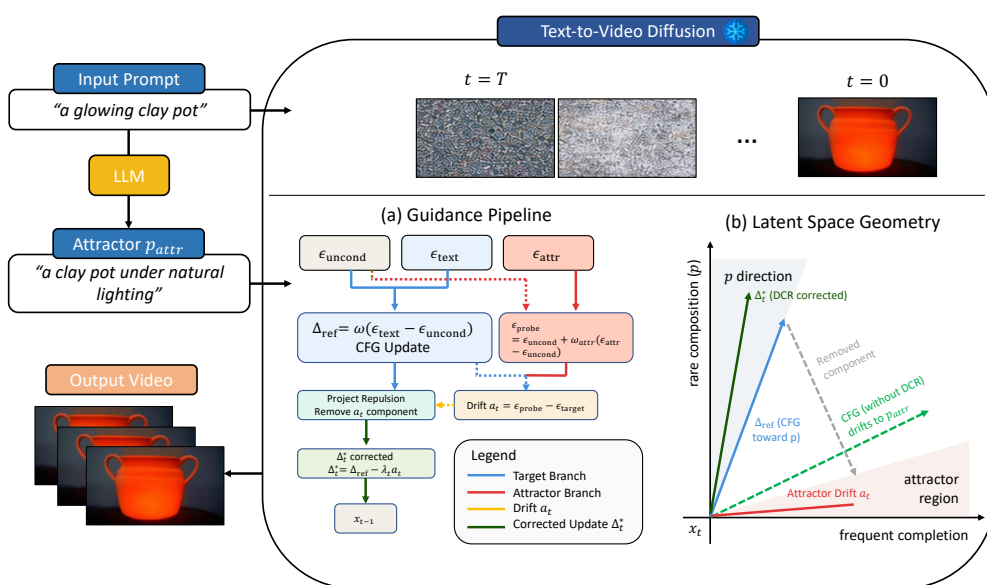


Figure 2: **Overview of Default Completion Repulsion (DCR)**. Given a rare but plausible compositional prompt  $p$  (e.g., “a glowing clay pot”), an LLM generates an attractor prompt  $p_{\text{attr}}$  representing the nearest frequent counterpart (e.g., “a clay pot under natural lighting”). Both prompts enter the text-to-video diffusion process, where DCR is applied at each denoising step. **(a) Guidance Pipeline:** Three denoiser branches are computed—unconditional  $\epsilon_{\text{uncond}}$ , text-conditioned  $\epsilon_{\text{text}}$ , and attractor-conditioned  $\epsilon_{\text{attr}}$ . The standard CFG update is defined as  $\Delta_{\text{ref}} = w(\epsilon_{\text{text}} - \epsilon_{\text{uncond}})$ . An attractor probe  $\epsilon_{\text{probe}} = \epsilon_{\text{uncond}} + w_{\text{attr}}(\epsilon_{\text{attr}} - \epsilon_{\text{uncond}})$  is constructed using a reduced guidance scale  $w_{\text{attr}} < w$ , and the counterfactual attractor drift is defined as  $a_t = \epsilon_{\text{probe}} - \epsilon_{\text{target}}$ . A projection-based repulsion mechanism removes the component of  $\Delta_{\text{ref}}$  aligned with  $a_t$ , yielding the corrected update  $\Delta_t^* = \Delta_{\text{ref}} - \lambda_t a_t$ . **(b) Latent Space Geometry:** Standard CFG drifts toward the attractor region (frequent completion  $p_{\text{attr}}$ ), while DCR redirects the denoising trajectory toward the rare composition direction  $p$  by removing the attractor-aligned component from the guidance update. The resulting trajectory produces compositionally faithful video generation without retraining the backbone diffusion model.

energy-based constrained generation [47], multi-objective scheduling [44], and constrained diffusion for safe control [48]. Despite their effectiveness, these methods rescale or reweight the conditional signal without modeling competing semantic directions. They do not account for *implicit attractors* induced by the training distribution, which bias generation toward frequent configurations. In contrast, our approach explicitly identifies default completion tendencies and applies targeted repulsive guidance.

## 2.2 Compositional and Negation-Based Generation

Generating outputs that faithfully combine multiple semantic concepts remains a central challenge [36, 46, 21]. Composable Diffusion [25], Attend-and-Excite [7], Structured Diffusion [9], and linguistic binding [29] improve multi-concept consistency, but primarily address conflicts between specified concepts rather than the model’s tendency to favor frequent alternatives. Vision-language models are known to struggle with negation [2, 49, 35, 43], and concept erasure methods suppress specific concepts via weight modification [10, 11]. The closest prior work, NEGATE [22], uses contrastive guidance to enforce *explicit* negation constraints stated in the prompt; we adapt its attractor-directed metric analogues in Sec. 4.4. DCR instead targets *implicit* default completion tendencies that arise without any explicit constraint, and replaces unconditional contrastive subtraction with projection-based repulsion on the guidance update.

## 2.3 Diffusion Models for Image and Video Generation

Denoising diffusion [17] and latent diffusion models [30] underpin scalable text-to-image generation. This framework has been extended to video synthesis across diverse architectures [19, 6, 5, 16, 34, 4, 13, 24, 40, 39, 15, 28, 14, 20, 38, 12, 41], including closed-source systems such as Sora [26], Veo [32], Veo 2 [37], and Movie Gen [27]. Recent open models including CogVideoX [45], HunyuanVideo [42, 23], and Mochi [1] further advance quality and temporal consistency. Despite these advances, pretrained models inherit distributional biases that manifest as *default completion* behavior, drifting toward high-frequency patterns even for valid rare compositions. Our work introduces a training-free mechanism that detects and counteracts such attractors at inference time.

### 3 Method

#### 3.1 Problem Setup

Let  $x_t \in \mathbb{R}^{C \times F \times H \times W}$  denote the latent variable at diffusion step  $t$ . Given a prompt  $p$  describing a rare but plausible composition, our goal is to prevent the denoising trajectory from collapsing toward a more frequent completion favored by the pretrained model.

We denote the denoiser prediction by

$$\epsilon_\theta(x_t, t, p),$$

and the unconditional branch by

$$\epsilon_{\text{uncond}} := \epsilon_\theta(x_t, t, \emptyset).$$

Under standard classifier-free guidance (CFG), the guided update is

$$\Delta_{\text{ref}} = w (\epsilon_{\text{text}} - \epsilon_{\text{uncond}}), \quad (1)$$

where

$$\epsilon_{\text{text}} := \epsilon_\theta(x_t, t, p),$$

and  $w > 1$  is the guidance scale. The corresponding guided prediction is

$$\epsilon_{\text{target}} = \epsilon_{\text{uncond}} + \Delta_{\text{ref}}. \quad (2)$$

Our method augments this formulation with an additional branch that exposes a competing completion tendency under relaxed semantics.

#### 3.2 Attractor Prompt

We introduce an attractor prompt  $p_{\text{attr}}$  that represents a relaxed version of the original prompt  $p$ . Specifically,  $p_{\text{attr}}$  removes or weakens the rare compositional factor while preserving the surrounding semantic context.

For example, a prompt such as “a snowy beach” can be relaxed into a more common completion such as “a tropical beach.”

We define:

$$\epsilon_{\text{attr}} := \epsilon_\theta(x_t, t, p_{\text{attr}}).$$

**Interpretation.** The attractor prompt induces a counterfactual completion trajectory that reflects how the model tends to complete the scene when the rare constraint is relaxed.

#### 3.3 Counterfactual Probe Branch

We construct a probe branch using a reduced guidance scale:

$$\epsilon_{\text{probe}} = \epsilon_{\text{uncond}} + w_{\text{attr}} (\epsilon_{\text{attr}} - \epsilon_{\text{uncond}}), \quad (3)$$

where  $0 \leq w_{\text{attr}} < w$ .

**Role of  $w_{\text{attr}}$ .** The parameter  $w_{\text{attr}}$  controls the influence strength of the attractor branch independently of the semantic content of  $p_{\text{attr}}$ . This enables fine-grained adjustment of the attractor trajectory magnitude without modifying the attractor prompt itself, thereby avoiding additional semantic distortion. This branch is not used for final generation, but instead serves as a probe revealing a competing direction favored by the model.

#### 3.4 Counterfactual Attractor Drift

We define the attractor drift as:

$$a_t = \epsilon_{\text{probe}} - \epsilon_{\text{target}}. \quad (4)$$

Expanding:

$$a_t = w_{\text{attr}} (\epsilon_{\text{attr}} - \epsilon_{\text{uncond}}) - w (\epsilon_{\text{text}} - \epsilon_{\text{uncond}}). \quad (5)$$

Because  $p_{\text{attr}} \neq p$ , we have  $\epsilon_{\text{attr}} \neq \epsilon_{\text{text}}$  whenever the denoiser is sensitive to the relaxed compositional factor, so the two direction vectors  $\epsilon_{\text{attr}} - \epsilon_{\text{uncond}}$  and  $\epsilon_{\text{text}} - \epsilon_{\text{uncond}}$  are not collinear. Equivalently,  $a_t$  cannot be written as  $c (\epsilon_{\text{text}} - \epsilon_{\text{uncond}})$  for any scalar  $c$ . This distinguishes our update from any guidance-scale rescaling  $\Delta_{\text{ref}} \mapsto c \Delta_{\text{ref}}$ , which only modulates *magnitude* along a fixed direction; the projection in Sec. 3.6 therefore removes a genuinely distinct completion tendency rather than merely attenuating the guidance strength.

### 3.5 Scheduled Repulsion

Let  $i$  denote the current step and  $T$  the total number of steps:

$$\pi_t = \frac{i}{T-1}. \quad (6)$$

Repulsion is activated only when

$$r_s \leq \pi_t \leq r_e. \quad (7)$$

Within this interval:

$$\tilde{\pi}_t = \text{clip}\left(\frac{\pi_t - r_s}{r_e - r_s}, 0, 1\right), \quad (8)$$

$$\alpha_t = \tilde{\pi}_t^\gamma. \quad (9)$$

Outside this interval,  $\alpha_t = 0$ .

### 3.6 Projection-Based Repulsion

We flatten:

$$\bar{a}_t = \text{vec}(a_t), \quad \bar{\Delta}_{\text{ref}} = \text{vec}(\Delta_{\text{ref}}). \quad (10)$$

Compute:

$$s_t = \bar{a}_t^\top \bar{\Delta}_{\text{ref}}, \quad (11)$$

$$n_t = \|\bar{a}_t\|_2^2 + \varepsilon. \quad (12)$$

We define:

$$\lambda_t = \alpha_t \eta \frac{\max(s_t, 0)}{n_t}. \quad (13)$$

The corrected update and final denoising step are:

$$\Delta_t^* = \Delta_{\text{ref}} - \lambda_t a_t, \quad (14)$$

$$\epsilon_t^* = \epsilon_{\text{uncond}} + \Delta_t^*, \quad (15)$$

$$x_{t-1} = \text{SchedulerStep}(\epsilon_t^*, t, x_t). \quad (16)$$

**Interpretation.** This correction removes only the component of the CFG update that aligns with the attractor direction, preventing collapse toward frequent completions while preserving other semantic components.

## 4 Experiments and Results

### 4.1 Implementation Details

Our method is implemented as a guidance-augmented inference procedure within the standard diffusion sampling loop, without modifying or retraining the backbone model. During classifier-free guidance, we compute three prediction branches: unconditional, text-conditioned, and an attractor-conditioned branch derived from the transformed prompt  $p_{\text{attr}}$ . Instead of directly subtracting the attractor prediction, we interpret default completion bias as a soft directional constraint on the guidance update and perform a projection-based correction that removes the component of the CFG direction aligned with the attractor drift. The repulsion strength follows a polynomial schedule  $\alpha_t = \tilde{\pi}_t^\gamma$  with  $\gamma = 2.0$ , gradually increasing suppression of the attractor direction over the active interval. Only positive alignment between the attractor drift and the CFG update is penalized, and numerical stabilization uses  $\varepsilon = 10^{-8}$ . All backbone-specific parameters follow default configurations [1], and no additional learnable parameters are introduced. We use Mochi as the primary backbone since it exposes a clean three-branch CFG interface for controlled ablation; the formulation is backbone-invariant by construction, and the targeted failure mode is shared across HunyuanVideo [23] and CogVideoX [45] (Sec. 4.3, Appendix H).



“a glowing clay pot”

Figure 3: **Representative qualitative comparison (ATTR)**. We compare our method with state-of-the-art diffusion baselines (Mochi, HunyuanVideo, CogVideoX) on Attribute Rebinding (ATTR): “a glowing clay pot.” While baselines often alter object identity or material properties (e.g., generating molten objects or unrelated glowing containers), our method correctly binds the luminous attribute to the clay pot, preserving both object identity and material consistency.

## 4.2 Benchmarking Datasets

Standard vision-language benchmarks are **insufficient for evaluating rare compositional generation**. Existing datasets such as MS-COCO, CC, or WebVid are designed for caption alignment and semantic similarity, rather than assessing the *distributional behavior of generated samples* under compositional constraints. Rare compositions are **underrepresented and not systematically controlled**, and these datasets do not capture the model’s tendency to drift toward more frequent alternatives during generation. To address this limitation, we construct a controlled evaluation suite specifically designed to probe *compositional fidelity* in diffusion models. Unlike representation-based evaluation, which measures alignment (e.g.,  $S(I, T)$ ), our objective is inherently generative:

$$\mathbb{P}_{x_0 \sim p_\theta(\cdot|p)} [\mathcal{C}(x_0; p) = 1], \quad (17)$$

where  $\mathcal{C}(x_0; p)$  denotes whether the generated sample satisfies the compositional constraint specified by prompt  $p$ . The benchmark consists of eight complementary categories (ENV, TEMP, OBJ, ATTR, SCALE, CTX, MAT, DENS), each targeting a distinct compositional factor such as environment recombination, temporal misalignment, object-context mismatch, attribute binding, scale variation, contextual relocation, material-state conflict, and density control. Each category contains 50 carefully designed prompts (400 total), with all prompts constructed to be **physically plausible yet distributionally rare**. Rather than maximizing prompt volume, the dataset prioritizes **controlled rarity, failure isolation, and semantic precision**, ensuring that each prompt induces a targeted conflict between the intended composition and the model’s learned prior. This enables systematic analysis of *compositional collapse*, where generated samples deviate toward high-probability alternatives despite valid prompt specifications. The dataset is used exclusively for evaluation; no training or fine-tuning is performed. **Detailed dataset construction, category definitions, and examples are provided in Appendix B.**

## 4.3 Qualitative Results

Figure 3 presents a representative qualitative comparison on the ATTR category. **Extended comparisons across all eight compositional categories are provided in Appendix C.** Baseline models exhibit a consistent failure mode across all categories: the denoising trajectory collapses toward the most statistically dominant completion, ignoring one or both compositional factors. In ENV, baselines render *a snowy beach with waves* as a standard tropical beach. In TEMP, *a rainbow at night* elicits daytime rainbow generations from Mochi and HunyuanVideo, while CogVideoX produces a fully

Method	CLIPScore $\uparrow$	CLIP-attr $\downarrow$	BLIP $\uparrow$	CCS $\uparrow$	CVR $\downarrow$
Mochi	0.3040	0.2718	0.7807	3.8375	0.4725
HunyuanVideo	0.3067	0.2725	0.7819	3.9750	0.3750
CogVideoX	0.2858	0.2644	0.7290	3.1925	0.5175
<b>Ours</b>	<b>0.3131</b>	<b>0.2558</b>	<b>0.8075</b>	<b>4.1300</b>	<b>0.3100</b>
Negative Prompt	0.2735	0.2610	0.7065	3.0375	0.4375
Ours w/o Attractor Prompt	0.3088	0.2709	0.7794	3.9275	0.3400
Ours w/o Repulsion	0.3088	0.2732	0.7729	3.9500	0.3475
Ours w/o Schedule	0.3115	0.2740	0.7819	3.9675	0.3550

Table 1: **Quantitative evaluation results.** All metrics are averaged over the full evaluation set. Mochi, HunyuanVideo, and CogVideoX denote standard CFG baselines. Negative Prompt denotes the baseline where  $p_{\text{attr}}$  is provided as a negative prompt within standard CFG on Mochi. Ablation variants are based on Mochi. CCS denotes the Compositional Compliance Score and CVR denotes the Compositional Violation Rate, both obtained from a GPT-4o vision-language judge.

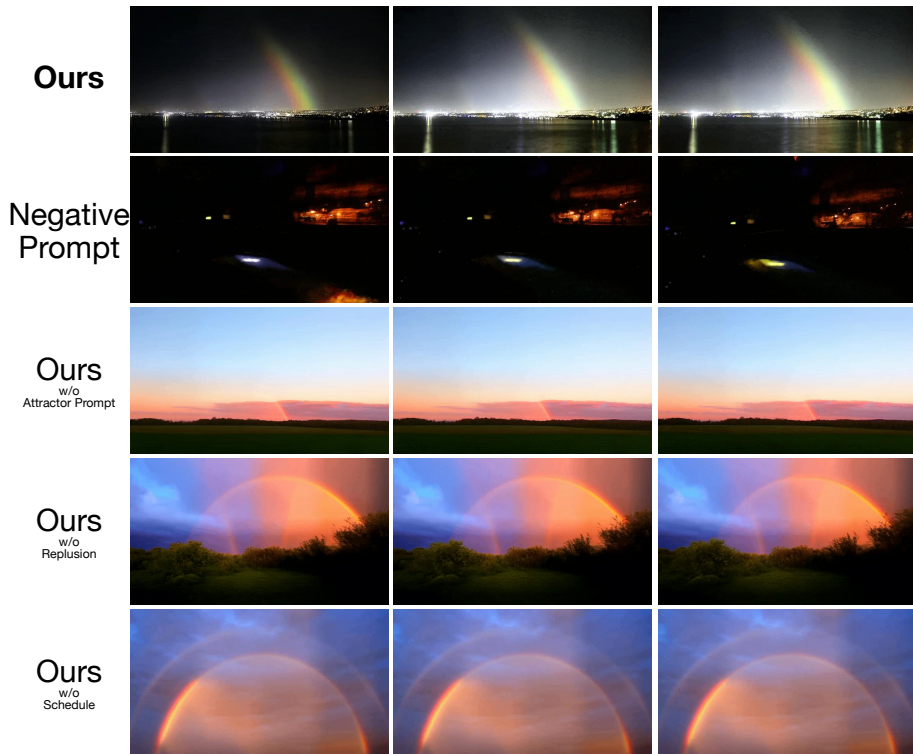
dark frame. In OBJ and CTX, objects and scenes revert to their most common contexts. In SCALE and MAT, baselines ignore scale constraints and simplify physically inconsistent states to a single dominant mode. Our method applies projection-based repulsion along the counterfactual attractor direction at each denoising step, preventing collapse while preserving other semantic components. As shown in Figure 3, DCR correctly binds the luminous attribute to the clay pot, maintaining both object identity and material consistency. This pattern holds consistently across all eight categories, confirming that DCR enables reliable generation of rare but semantically valid compositions.

#### 4.4 Quantitative Evaluation

We evaluate compositional generation using standard, widely adopted metrics without modifying prompts or introducing threshold-based rules. Our evaluation measures (1) global prompt alignment, (2) attractor suppression, and (3) compositional realization at both embedding and reasoning levels. Global alignment is measured using CLIPScore between generated frames and the full textual prompt  $p$ , which specifies the intended rare composition. Attractor suppression is quantified via CLIP similarity to the attractor prompt  $p_{\text{attr}}$  (CLIP-attr), where lower values indicate stronger resistance to default completion tendencies. We further compute BLIP-based caption similarity to evaluate text-level semantic fidelity, providing a complementary measure of compositional consistency based on generated descriptions rather than direct image-text alignment. Together, CLIPScore, CLIP-attr, and BLIP capture (1) alignment with the intended composition, (2) suppression of frequent alternatives, and (3) semantic consistency across modalities. To complement embedding-based evaluation, we additionally introduce two direct vision-language metrics: the *Compositional Compliance Score (CCS)* and the *Compositional Violation Rate (CVR)*. CCS is obtained from a multimodal language model that directly reasons over sampled video frames and assigns a 1–5 compliance score based on whether both compositional factors are simultaneously present and coherently realized. CVR measures the empirical frequency of attractor-driven collapse, i.e., cases where the generated output reflects the frequent counterpart rather than the intended rare composition. These metrics evaluate compositional fidelity at the semantic reasoning level rather than within embedding space. All results are averaged over our structured benchmark. As shown in Table 1, our method achieves the best performance across all metrics, improving CLIPScore (0.3131) while reducing CLIP-attr (0.2558), thereby achieving stronger alignment with the intended composition and better suppression of attractor bias without trade-offs. It also attains the highest BLIP score (0.8075), indicating improved semantic consistency. More importantly, our method significantly improves reasoning-level metrics, achieving the highest CCS (4.13) and the lowest CVR (0.31), with substantial reductions in compositional collapse compared to Mochi and Negative Prompt baselines. These results confirm that our approach effectively prevents compositional collapse and enables reliable generation of rare but semantically valid configurations. **More quantitative analysis is provided in Appendix D.**

#### 4.5 Ablation Study

We ablate four design choices: (i) the attractor prompt  $p_{\text{attr}}$ , (ii) the repulsion update, (iii) constraint scheduling, and (iv) a negative prompt baseline. As shown in Table 2, substituting  $p_{\text{attr}}$  as a standard CFG negative prompt most severely degrades performance, reducing CLIPScore to 0.2735 and BLIP to 0.7065; as visible in Figure 4, the generated frames are near-black and featureless, confirming that unconditional CFG repulsion suppresses not only the unwanted attribute but the broader semantic content required for the rare composition. Removing the attractor prompt collapses the probe branch onto the main guidance direction, eliminating any meaningful drift estimate; the model reverts to a



“a rainbow at night in the sky”

Figure 4: **Ablation study on rare compositional generation.** We compare our full model against four ablations on the prompt “a rainbow at night in the sky.” **Negative Prompt** replaces the attractor prompt  $p_{\text{attr}}$  into the negative slot of standard CFG, producing dark, near-black frames that entirely fail to render the rainbow—confirming that naive negation via CFG cannot encode compositional rarity. **w/o Attractor Prompt** collapses the probe branch onto the main prompt  $p$ , reducing guidance to a scale-relaxation baseline; the model defaults to a daytime sky, demonstrating that a semantically distinct  $p_{\text{attr}}$  is essential for identifying the drift direction. **w/o Repulsion** retains the attractor probe but sets  $\lambda_t = 0$ , disabling the projection-based correction; the output drifts toward a common daylight rainbow, confirming that the repulsion update is the operative mechanism for suppressing model-prior bias. **w/o Schedule** applies repulsion uniformly ( $\alpha_t = 1$ ) across all denoising steps; early-step interference disrupts global structure formation, yielding an oversaturated close-up arc that loses the intended nocturnal scene context. Our full model correctly synthesizes a rainbow against a dark night sky while maintaining temporal coherence across frames.

prototypical daytime sky (Figure 4), with CLIP-attr rising to 0.2709 and CVR increasing to 0.3400. Disabling the repulsion update while retaining the probe yields the largest increase in CLIP-attr (0.2732), and the output drifts toward the model’s high-probability prior despite the drift direction being correctly identified, confirming that the corrective projection is the operative suppression mechanism. Removing constraint scheduling produces the highest CVR (0.3550) despite a relatively preserved CLIPScore; as shown in Figure 4, premature repulsion during early denoising steps corrupts global structure, yielding an oversaturated close-up arc that loses nocturnal scene context. Both ablations on the repulsion mechanism reduce CCS and increase CVR under vision-language evaluation, confirming genuine compositional violations. **More detailed analysis is provided in Appendix E.**

#### 4.6 Attractor Trajectory Visualization

Figure 5 (left) compares videos generated by Ours (DCR), Mochi (standard CFG baseline), and  $p_{\text{attr}}$  only for a *snowy beach with waves*. The  $p_{\text{attr}}$ -only output closely resembles the Mochi baseline, both producing a snow-free sunny beach, confirming that  $p_{\text{attr}}$  accurately captures the model’s default completion tendency. This validates the core motivation of DCR: by explicitly modeling the attractor direction, the method can apply targeted repulsion to prevent compositional collapse. Extended comparisons across additional categories are provided in Appendix F.

#### 4.7 Hyperparameter Sensitivity

Figure 5 (right) reports the sensitivity of our method to three key hyperparameters: the attractor guidance scale  $w_{\text{attr}}$ , the repulsion strength  $\eta$ , and the schedule interval  $(r_s, r_e)$ . Across all three sweeps, CLIPScore and CLIP-attr remain stable within a variation of approximately 0.01, indicating that DCR does not require careful hyperparameter tuning to achieve effective attractor suppression. BLIP shows a mild monotonic trend with respect to  $w_{\text{attr}}$  and  $\eta$ , but remains competitive across all evaluated settings. For the schedule interval, the [0.2, 0.8] and [0.5, 1.0] configurations both perform

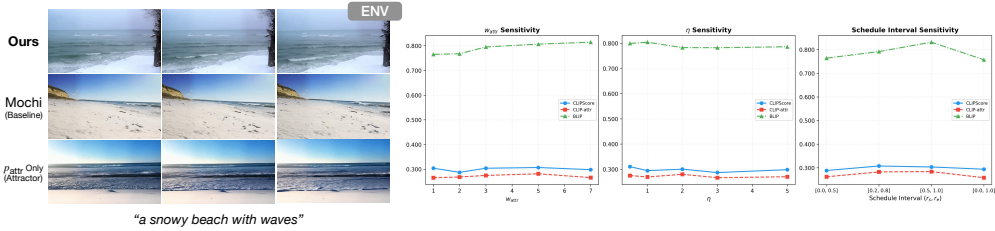


Figure 5: **Attractor trajectory visualization and hyperparameter sensitivity.** (Left) Comparison of Ours (DCR), Mochi (baseline), and  $p_{\text{attr}}$  only (attractor) for *a snowy beach with waves* (ENV). The  $p_{\text{attr}}$ -only output closely resembles the Mochi baseline, confirming that  $p_{\text{attr}}$  captures the model’s default completion tendency. (Right) Sensitivity of CLIPScore, CLIP-attr, and BLIP to  $w_{\text{attr}}$ ,  $\eta$ , and schedule interval  $(r_s, r_e)$ . All three metrics remain stable across a wide range of values, demonstrating that DCR does not require careful hyperparameter tuning.

well on embedding-based metrics, while our default  $[0.2, 0.8]$  provides a favorable balance between early structural formation and late-stage attractor suppression. These results confirm that DCR is robust to hyperparameter variation across a wide range of values, and that our default configuration ( $w_{\text{attr}} = 3.0$ ,  $\eta = 1.0$ ,  $(r_s, r_e) = [0.2, 0.8]$ ) reliably achieves strong compositional fidelity without exhaustive tuning.

## 5 Conclusions, Limitations and Future Work

This work presents the first explicit formulation of *default completion bias* as a generative failure mode in diffusion models. While prior studies have addressed compositional generation through stronger conditioning or attention manipulation, the intrinsic tendency of pretrained models to drift toward high-frequency semantic configurations has not previously been modeled as part of the generative process itself. We shift the perspective from reinforcing the target signal to explicitly identifying and suppressing competing completion tendencies, modeling default completion bias as a structured directional constraint over the denoising trajectory. Our formulation provides a unified treatment of diverse compositional failure modes—including environment recomposition, temporal misalignment, object-context mismatch, attribute rebinding, scale deviation, contextual relocation, material-state conflict, and density variation—within a single repulsion-based framework. Rather than introducing new architectures or retraining large models, we demonstrate how implicit distributional attractors can be revealed through counterfactual prompt relaxation and translated into geometric corrections on guidance update directions, enabling reliable generation of rare but semantically valid compositions. Importantly, this perspective extends naturally beyond rare compositional generation. Because repulsion is enforced at the level of denoising trajectory dynamics, the formulation applies to both image and video generation and suggests broader extensions toward controllable generation under distributional constraints. By treating default completion bias as a principled semantic operator rather than a prompt engineering problem, we establish a new research direction at the intersection of distributional generalization and neural generative modeling. This work positions implicit attractor suppression—not stronger conditioning—as a central challenge for next-generation controllable diffusion systems.

**Limitations & Future Work.** Our current formulation approximates default completion bias through a counterfactual attractor prompt  $p_{\text{attr}}$ , which requires identifying a semantically meaningful frequent counterpart for each target composition. While we automate this via LLM-based prompt relaxation, cases where the attractor is ambiguous or difficult to define precisely may limit suppression effectiveness. Additionally, the projection-based repulsion operates at the level of global latent directions and may not fully capture spatially localized or temporally varying compositional constraints. DCR is validated on Mochi as a single-backbone setting that allows clean attribution of the attractor probe, the projection-based repulsion, and the polynomial schedule; the formulation is invariant to backbone architecture by construction, and Appendix H discusses this scope together with the empirical observation, drawn from our comparisons against HunyuanVideo and CogVideoX, that compositional collapse is shared across the current generation of text-to-video diffusion models. Future work may extend this formulation to broader classes of distributional constraints beyond rare co-occurrence, including negation, quantification, and relational compositional structure. Integrating learned attractor estimation—rather than prompt-based relaxation—with neural trajectory control could further reduce dependence on explicit attractor specification. More broadly, viewing default completion suppression as a general principle for inference-time distributional correction opens new directions for controllable generation in image, video, and vision-language-action systems.

## References

- [1] Genmo AI. Mochi-1 preview. <https://huggingface.co/genmo/mochi-1-preview>, October 2024.
- [2] Kumail Alhamoud, Shaden Alshammari, Yonglong Tian, Guohao Li, Philip HS Torr, Yoon Kim, and Marzyeh Ghassemi. Vision-language models do not understand negation. In *Proceedings of the Computer Vision and Pattern Recognition Conference*, pages 29612–29622, 2025.
- [3] Arpit Bansal, Hong-Min Chu, Avi Schwarzschild, Soumyadip Sengupta, Micah Goldblum, Jonas Geiping, and Tom Goldstein. Universal guidance for diffusion models. In *Proceedings of the IEEE/CVF conference on computer vision and pattern recognition*, pages 843–852, 2023.
- [4] Omer Bar-Tal, Hila Chefer, Omer Tov, Charles Herrmann, Roni Paiss, Shiran Zada, Ariel Ephrat, Junhwa Hur, Guanghui Liu, Amit Raj, et al. Lumiere: A space-time diffusion model for video generation. In *SIGGRAPH Asia 2024 Conference Papers*, pages 1–11, 2024.
- [5] Andreas Blattmann, Tim Dockhorn, Sumith Kulal, Daniel Mendelevitch, Maciej Kilian, Dominik Lorenz, Yam Levi, Zion English, Vikram Voleti, Adam Letts, et al. Stable video diffusion: Scaling latent video diffusion models to large datasets. *arXiv preprint arXiv:2311.15127*, 2023.
- [6] Andreas Blattmann, Robin Rombach, Huan Ling, Tim Dockhorn, Seung Wook Kim, Sanja Fidler, and Karsten Kreis. Align your latents: High-resolution video synthesis with latent diffusion models. In *Proceedings of the IEEE/CVF conference on computer vision and pattern recognition*, pages 22563–22575, 2023.
- [7] Hila Chefer, Yuval Alaluf, Yael Vinker, Lior Wolf, and Daniel Cohen-Or. Attend-and-excite: Attention-based semantic guidance for text-to-image diffusion models. *ACM transactions on Graphics (TOG)*, 42(4):1–10, 2023.
- [8] Hyungjin Chung, Jeongsol Kim, Geon Yeong Park, Hyelin Nam, and Jong Chul Ye. Cfg++: Manifold-constrained classifier free guidance for diffusion models. *arXiv preprint arXiv:2406.08070*, 2024.
- [9] Weixi Feng, Xuehai He, Tsu-Jui Fu, Varun Jampani, Arjun Akula, Pradyumna Narayana, Sugato Basu, Xin Eric Wang, and William Yang Wang. Training-free structured diffusion guidance for compositional text-to-image synthesis. *arXiv preprint arXiv:2212.05032*, 2022.
- [10] Rohit Gandikota, Joanna Materzynska, Jaden Fiotto-Kaufman, and David Bau. Erasing concepts from diffusion models. In *Proceedings of the IEEE/CVF international conference on computer vision*, pages 2426–2436, 2023.
- [11] Rohit Gandikota, Hadas Orgad, Yonatan Belinkov, Joanna Materzyńska, and David Bau. Unified concept editing in diffusion models. In *Proceedings of the IEEE/CVF winter conference on applications of computer vision*, pages 5111–5120, 2024.
- [12] Songwei Ge, Seungjun Nah, Guilin Liu, Tyler Poon, Andrew Tao, Bryan Catanzaro, David Jacobs, Jia-Bin Huang, Ming-Yu Liu, and Yogesh Balaji. Preserve your own correlation: A noise prior for video diffusion models. In *Proceedings of the IEEE/CVF International Conference on Computer Vision*, pages 22930–22941, 2023.
- [13] Rohit Girdhar, Mannat Singh, Andrew Brown, Quentin Duval, Samaneh Azadi, Sai Saketh Rambhatla, Akbar Shah, Xi Yin, Devi Parikh, and Ishan Misra. Emu video: Factorizing text-to-video generation by explicit image conditioning. *arXiv preprint arXiv:2311.10709*, 2023.
- [14] Yingqing He, Tianyu Yang, Yong Zhang, Ying Shan, and Qifeng Chen. Latent video diffusion models for high-fidelity long video generation. *arXiv preprint arXiv:2211.13221*, 2022.
- [15] Roberto Henschel, Levon Khachatryan, Daniil Hayrapetyan, Hayk Poghosyan, Vahram Tadevosyan, Zhangyang Wang, Shant Navasardyan, and Humphrey Shi. Streamingt2v: Consistent, dynamic, and extendable long video generation from text. *arXiv preprint arXiv:2403.14773*, 2024.
- [16] Jonathan Ho, William Chan, Chitwan Saharia, Jay Whang, Ruiqi Gao, Alexey Gritsenko, Diederik P Kingma, Ben Poole, Mohammad Norouzi, David J Fleet, et al. Imagen video: High definition video generation with diffusion models. *arXiv preprint arXiv:2210.02303*, 2022.
- [17] Jonathan Ho, Ajay Jain, and Pieter Abbeel. Denoising diffusion probabilistic models. *Advances in neural information processing systems*, 33:6840–6851, 2020.
- [18] Jonathan Ho and Tim Salimans. Classifier-free diffusion guidance. *arXiv preprint arXiv:2207.12598*, 2022.

- [19] Jonathan Ho, Tim Salimans, Alexey Gritsenko, William Chan, Mohammad Norouzi, and David J Fleet. Video diffusion models. *Advances in neural information processing systems*, 35:8633–8646, 2022.
- [20] Wenyi Hong, Ming Ding, Wendi Zheng, Xinghan Liu, and Jie Tang. Cogvideo: Large-scale pretraining for text-to-video generation via transformers. *arXiv preprint arXiv:2205.15868*, 2022.
- [21] Cheng-Yu Hsieh, Jieyu Zhang, Zixian Ma, Aniruddha Kembhavi, and Ranjay Krishna. Sugarcrepe: Fixing hackable benchmarks for vision-language compositionality. *Advances in neural information processing systems*, 36:31096–31116, 2023.
- [22] Taewon Kang and Ming C Lin. Negate: Constrained semantic guidance for linguistic negation in text-to-video diffusion. *arXiv preprint arXiv:2603.06533*, 2026.
- [23] Weijie Kong, Qi Tian, Zijian Zhang, Rox Min, Zuozhuo Dai, Jin Zhou, Jiangfeng Xiong, Xin Li, Bo Wu, Jianwei Zhang, et al. Hunyuanvideo: A systematic framework for large video generative models. *arXiv preprint arXiv:2412.03603*, 2024.
- [24] Long Lian, Baifeng Shi, Adam Yala, Trevor Darrell, and Boyi Li. Llm-grounded video diffusion models. *arXiv preprint arXiv:2309.17444*, 2023.
- [25] Nan Liu, Shuang Li, Yilun Du, Antonio Torralba, and Joshua B Tenenbaum. Compositional visual generation with composable diffusion models. In *European conference on computer vision*, pages 423–439. Springer, 2022.
- [26] OpenAI. Video generation models as world simulators. <https://openai.com/index/video-generation-models-as-world-simulators/>, February 2024.
- [27] Adam Polyak, Amit Zohar, Andrew Brown, Andros Tjandra, Animesh Sinha, Ann Lee, Apoorv Vyas, Bowen Shi, Chih-Yao Ma, Ching-Yao Chuang, David Yan, Dhruv Choudhary, DingKang Wang, Geet Sethi, Guan Pang, Haoyu Ma, Ishan Misra, Ji Hou, Jialiang Wang, Kiran Jagadeesh, Kunpeng Li, Luxin Zhang, Mannat Singh, Mary Williamson, Matt Le, Matthew Yu, Mitesh Kumar Singh, Peizhao Zhang, Peter Vajda, Quentin Duval, Rohit Girdhar, Roshan Sumbaly, Sai Saketh Rambhatla, Sam Tsai, Samaneh Azadi, Samyak Datta, Sanyuan Chen, Sean Bell, Sharadh Ramaswamy, Shelly Sheynin, Siddharth Bhattacharya, Simran Motwani, Tao Xu, Tianhe Li, Tingbo Hou, Wei-Ning Hsu, Xi Yin, Xiaoliang Dai, Yaniv Taigman, Yaqiao Luo, Yen-Cheng Liu, Yi-Chiao Wu, Yue Zhao, Yuval Kirstain, Zecheng He, Zijian He, Albert Pumarola, Ali Thabet, Arsiom Sanakoyeu, Arun Mallya, Baishan Guo, Boris Araya, Breana Kerr, Carleigh Wood, Ce Liu, Cen Peng, Dimitry Vengertsev, Edgar Schonfeld, Elliot Blanchard, Felix Juefei-Xu, Fraylie Nord, Jeff Liang, John Hoffman, Jonas Kohler, Kaolin Fire, Karthik Sivakumar, Lawrence Chen, Licheng Yu, Luya Gao, Markos Georgopoulos, Rashel Moritz, Sara K. Sampson, Shikai Li, Simone Parmeggiani, Steve Fine, Tara Fowler, Vladan Petrovic, and Yuming Du. Movie gen: A cast of media foundation models, 2025.
- [28] Haonan Qiu, Menghan Xia, Yong Zhang, Yingqing He, Xintao Wang, Ying Shan, and Ziwei Liu. Freenoise: Tuning-free longer video diffusion via noise rescheduling. *arXiv preprint arXiv:2310.15169*, 2023.
- [29] Royi Rassin, Eran Hirsch, Daniel Glickman, Shauli Ravfogel, Yoav Goldberg, and Gal Chechik. Linguistic binding in diffusion models: Enhancing attribute correspondence through attention map alignment. *Advances in Neural Information Processing Systems*, 36:3536–3559, 2023.
- [30] Robin Rombach, Andreas Blattmann, Dominik Lorenz, Patrick Esser, and Björn Ommer. High-resolution image synthesis with latent diffusion models. In *Proceedings of the IEEE/CVF conference on computer vision and pattern recognition*, pages 10684–10695, 2022.
- [31] Chitwan Saharia, William Chan, Saurabh Saxena, Lala Li, Jay Whang, Emily L Denton, Kamyar Ghasemipour, Raphael Gontijo Lopes, Burcu Karagol Ayan, Tim Salimans, et al. Photorealistic text-to-image diffusion models with deep language understanding. *Advances in neural information processing systems*, 35:36479–36494, 2022.
- [32] Abhishek Sharma, Adams Yu, Ali Razavi, Andeep Toor, Andrew Pierson, Ankush Gupta, Austin Waters, Aäron van den Oord, Daniel Tanis, Dumitru Erhan, Eric Lau, Eleni Shaw, Gabe Barth-Maron, Greg Shaw, Han Zhang, Henna Nandwani, Hernan Moraldo, Hyunjik Kim, Irina Blok, Jakob Bauer, Jeff Donahue, Junyoung Chung, Kory Mathewson, Kurtis David, Lasse Espeholt, Marc van Zee, Matt McGill, Medhini Narasimhan, Miaosen Wang, Mikołaj Bińkowski, Mohammad Babaeizadeh, Mohammad Taghi Saffar, Nando de Freitas, Nick Pezzotti, Pieter-Jan Kindermans, Poorva Rane, Rachel Hornung, Robert Riachi, Ruben Villegas, Rui Qian, Sander Dieleman, Serena Zhang, Serkan Cabi, Shixin Luo, Shlomi Fruchter, Signe Nørly, Srivatsan Srinivasan, Tobias Pfaff, Tom Hume, Vikas Verma, Weizhe Hua, William Zhu, Xinchun Yan, Xinyu Wang, Yelin Kim, Yuqing Du, and Yutian Chen. Veo. 2024.

- [33] Chenyang Si, Ziqi Huang, Yuming Jiang, and Ziwei Liu. Freeu: Free lunch in diffusion u-net. In *Proceedings of the IEEE/CVF conference on computer vision and pattern recognition*, pages 4733–4743, 2024.
- [34] Uriel Singer, Adam Polyak, Thomas Hayes, Xi Yin, Jie An, Songyang Zhang, Qiyuan Hu, Harry Yang, Oron Ashual, Oran Gafni, et al. Make-a-video: Text-to-video generation without text-video data. *arXiv preprint arXiv:2209.14792*, 2022.
- [35] Jaisidh Singh, Ishaan Shrivastava, Mayank Vatsa, Richa Singh, and Aparna Bharati. Learn" no" to say" yes" better: Improving vision-language models via negations. *arXiv preprint arXiv:2403.20312*, 2024.
- [36] Tristan Thrush, Ryan Jiang, Max Bartolo, Amanpreet Singh, Adina Williams, Douwe Kiela, and Candace Ross. Winoground: Probing vision and language models for visio-linguistic compositionality. In *Proceedings of the IEEE/CVF Conference on Computer Vision and Pattern Recognition*, pages 5238–5248, 2022.
- [37] Veo-Team, :, Agrim Gupta, Ali Razavi, Andeep Toor, Ankush Gupta, Dumitru Erhan, Eleni Shaw, Eric Lau, Frank Belletti, Gabe Barth-Maron, Gregory Shaw, Hakan Erdogan, Hakim Sidahmed, Henna Nandwani, Hernan Moraldo, Hyunjik Kim, Irina Blok, Jeff Donahue, José Lezama, Kory Mathewson, Kurtis David, Matthieu Kim Lorrain, Marc van Zee, Medhini Narasimhan, Miaosen Wang, Mohammad Babaeizadeh, Nelly Papalampidi, Nick Pezzotti, Nilpa Jha, Parker Barnes, Pieter-Jan Kindermans, Rachel Hornung, Ruben Villegas, Ryan Poplin, Salah Zaiem, Sander Dieleman, Sayna Ebrahimi, Scott Wisdom, Serena Zhang, Shlomi Fruchter, Signe Nørly, Weizhe Hua, Xinchun Yan, Yuqing Du, and Yutian Chen. Veo 2. 2024.
- [38] Ruben Villegas, Mohammad Babaeizadeh, Pieter-Jan Kindermans, Hernan Moraldo, Han Zhang, Mohammad Taghi Saffar, Santiago Castro, Julius Kunze, and Dumitru Erhan. Phenaki: Variable length video generation from open domain textual description. *arXiv preprint arXiv:2210.02399*, 2022.
- [39] Fu-Yun Wang, Wenshuo Chen, Guanglu Song, Han-Jia Ye, Yu Liu, and Hongsheng Li. Gen-l-video: Multi-text to long video generation via temporal co-denoising. *arXiv preprint arXiv:2305.18264*, 2023.
- [40] Jiuniu Wang, Hangjie Yuan, Dayou Chen, Yingya Zhang, Xiang Wang, and Shiwei Zhang. Modelscope text-to-video technical report. *arXiv preprint arXiv:2308.06571*, 2023.
- [41] Yaohui Wang, Xinyuan Chen, Xin Ma, Shangchen Zhou, Ziqi Huang, Yi Wang, Ceyuan Yang, Yinan He, Jiashuo Yu, Peiqing Yang, et al. Lavie: High-quality video generation with cascaded latent diffusion models. *International Journal of Computer Vision*, pages 1–20, 2024.
- [42] Bing Wu, Chang Zou, Changlin Li, Duojuan Huang, Fang Yang, Hao Tan, Jack Peng, Jianbing Wu, Jiangfeng Xiong, Jie Jiang, et al. Hunyuanvideo 1.5 technical report. *arXiv preprint arXiv:2511.18870*, 2025.
- [43] Junhao Xiao, Zhiyu Wu, Hao Lin, Yahui Liu, Xiaoran Zhao, Zixu Wang, Zejiang He, and Yi Chen. Not just what’s there: Enabling clip to comprehend negated visual descriptions without fine-tuning. In *Proceedings of the AAAI Conference on Artificial Intelligence (AAAI 2026)*. AAAI Press, January 2026. Main Conference.
- [44] Xin Xie and Dong Gong. Dymo: Training-free diffusion model alignment with dynamic multi-objective scheduling. In *Proceedings of the Computer Vision and Pattern Recognition Conference*, pages 13220–13230, 2025.
- [45] Zhuoyi Yang, Jiayan Teng, Wendi Zheng, Ming Ding, Shiyu Huang, Jiazheng Xu, Yuanming Yang, Wenyi Hong, Xiaohan Zhang, Guanyu Feng, et al. Cogvideox: Text-to-video diffusion models with an expert transformer. *arXiv preprint arXiv:2408.06072*, 2024.
- [46] Mert Yuksekogonul, Federico Bianchi, Pratyusha Kalluri, Dan Jurafsky, and James Zou. When and why vision-language models behave like bags-of-words, and what to do about it? *arXiv preprint arXiv:2210.01936*, 2022.
- [47] Stefano Zampini, Jacob K Christopher, Luca Oneto, Davide Anguita, and Ferdinando Fioretto. Training-free constrained generation with stable diffusion models. *arXiv preprint arXiv:2502.05625*, 2025.
- [48] Jichen Zhang, Liqun Zhao, Antonis Papachristodoulou, and Jack Umenberger. Constrained diffusers for safe planning and control. *arXiv preprint arXiv:2506.12544*, 2025.
- [49] Yuhui Zhang, Yuchang Su, Yiming Liu, and Serena Yeung-Levy. Negvqa: Can vision language models understand negation? In *Findings of the Association for Computational Linguistics: ACL 2025*, pages 3707–3716, 2025.

## A Ethics Statement

### Ethics Statement

This work introduces Default Completion Repulsion (DCR), a training-free inference-time guidance method for text-to-video diffusion models. We address the following ethical considerations. **Intended Use.** DCR is designed to improve compositional fidelity in generative video models by suppressing distributional biases that cause models to ignore rare but valid semantic combinations. The method is intended for research purposes and for applications where faithful prompt adherence is required, such as creative content generation, simulation, and visual prototyping. **Potential Misuse.** As with all generative video methods, DCR could in principle be applied to produce misleading, harmful, or deceptive content. We note that DCR does not introduce new generative capabilities beyond those of the underlying backbone model; it modifies guidance at inference time to better reflect the intended prompt. The risks associated with DCR are therefore no greater than those of the backbone diffusion models on which it operates. **Benchmark and Data.** The DCR-Bench evaluation suite is constructed solely for research evaluation purposes. All prompts are manually designed to be physically plausible and free of harmful, offensive, or privacy-violating content. No personally identifiable information is collected or used. The benchmark is released for reproducibility and to facilitate future research on compositional generation. **Computational Resources.** DCR operates entirely at inference time and requires no additional training. The primary computational overhead relative to standard CFG is a single additional denoiser forward pass per step for the attractor branch. All experiments were conducted on standard research GPU hardware. **Broader Impact.** By improving the ability of generative models to faithfully realize rare but valid compositions, DCR may contribute to more reliable and controllable AI-generated content. We hope this work encourages further research into distributional bias in generative models and inference-time methods for controllable generation.

## B Detailed Benchmarking Dataset

Unlike prior works that evaluate compositional generalization through retrieval or captioning accuracy, our objective is to assess *compositional fidelity in generative diffusion trajectories*. This distinction fundamentally changes the role of datasets in our evaluation protocol.

**Why Standard Datasets Are Insufficient.** Conventional vision-language benchmarks such as MS-COCO, CC, or WebVid are designed for descriptive captioning and semantic alignment. Rare compositional prompts are **underrepresented, unstructured, and not systematically controlled**. More importantly, these datasets evaluate **representation-level similarity** rather than the **distributional behavior of generated samples under compositional constraints**.

In representation learning settings, evaluation typically takes the form:

$$S(I, T_{\text{target}}) > S(I, T_{\text{distractor}}),$$

which measures embedding alignment. In contrast, our problem is generative and distributional:

$$\mathbb{P}_{x_0 \sim p_\theta(\cdot|p)} [\mathcal{C}(x_0; p) = 1], \quad (18)$$

where  $\mathcal{C}(x_0; p)$  denotes whether the generated sample satisfies the target composition specified by prompt  $p$ .

Standard datasets do not provide structured prompts to estimate Eq. (18), nor do they expose systematic deviations toward frequent alternatives. Therefore, we construct a controlled evaluation suite tailored to compositional fidelity.

**Dataset Scale.** We construct eight categories, each containing 50 prompts, resulting in a total of 400 evaluation samples. Each prompt is designed to isolate a specific compositional failure mode. The dataset is used solely for evaluation; no training or fine-tuning is performed.

**Compositional Constraint Formulation.** Each prompt  $p$  implicitly defines a compositional constraint over generated samples:

$$\mathcal{C}(x_0; p) = \prod_{k=1}^K \mathbf{1}[g_k(x_0) \in \mathcal{S}_k(p)], \quad (19)$$

where  $g_k(x_0)$  denotes a semantic factor (e.g., environment, object, scale), and  $\mathcal{S}_k(p)$  defines the allowable set specified by the prompt.

Compositional collapse occurs when

$$g_k(x_0) \notin \mathcal{S}_k(p), \quad (20)$$

typically drifting toward a high-probability alternative under the model prior:

$$g_k(x_0) \in \mathcal{S}_k^{\text{prior}}, \quad \mathcal{S}_k^{\text{prior}} \neq \mathcal{S}_k(p). \quad (21)$$

Our dataset is explicitly designed to induce such conflicts between target composition and prior preference.

**Design Principles.** The dataset is constructed under four key principles:

- **Physical Plausibility:** All prompts are visually realizable.
- **Controlled Rarity:** Prompts lie in low-density regions of  $p_\theta(x_0 | p)$ .
- **Failure Isolation:** Each category isolates a distinct semantic factor  $g_k$ .
- **Non-Triviality:** Prompts avoid degenerate solutions such as object removal.

### (1) ENV: Environment Recomposition

This category evaluates rare combinations of environmental factors:

“A snowy beach with waves.”  
 “A desert oasis surrounded by snow.”  
 “A lake shore with snow and blooming flowers.”

Here, the constraint applies to the environment factor:

$$g_{\text{env}}(x_0) \in \mathcal{S}_{\text{env}}(p),$$

where  $\mathcal{S}_{\text{env}}(p)$  includes atypical co-occurrences. Models often collapse toward a dominant single-environment mode.

### (2) TEMP: Temporal Misalignment

This category evaluates rare temporal and astronomical co-occurrences:

“A rainbow at night in the sky.”  
 “A sunrise with stars still visible in the sky.”  
 “A sunrise sky with a visible rainbow and moon together.”

The constraint is defined over temporal factors:

$$g_{\text{time}}(x_0) \in \mathcal{S}_{\text{time}}(p),$$

which conflicts with learned time-of-day priors.

### (3) OBJ: Object Relocation

This category evaluates object-environment mismatches:

“A lighthouse located in a grassy meadow.”  
 “A canoe placed in a dry canyon.”  
 “A surfboard standing in a grassy field.”

We require:

$$(g_{\text{obj}}(x_0), g_{\text{env}}(x_0)) \in \mathcal{S}_{\text{joint}}(p),$$

where the joint configuration is rare but valid.

#### (4) ATTR: Attribute Rebinding

This category evaluates unusual attribute-material bindings:

“A glowing clay pot.”  
“A reflective wooden table like a mirror.”  
“A solid cloud shaped like a rock.”

The constraint operates on attribute consistency:

$$g_{\text{attr}}(x_0) \in \mathcal{S}_{\text{attr}}(p),$$

which may conflict with learned material priors.

#### (5) SCALE: Scale Shift

This category evaluates deviations in object scale:

“A giant cat larger than a building.”  
“A tiny chair placed on a finger.”  
“A tiny bench on a coin.”

The constraint is:

$$g_{\text{scale}}(x_0) \in \mathcal{S}_{\text{scale}}(p),$$

which often conflicts with typical size distributions.

#### (6) CTX: Contextual Relocation

This category evaluates unusual scene placement:

“A kitchen in the middle of a highway.”  
“A library on a beach.”  
“A restaurant dining area in the middle of a highway.”

The constraint is defined over context:

$$g_{\text{ctx}}(x_0) \in \mathcal{S}_{\text{ctx}}(p),$$

which competes with strong context priors.

#### (7) MAT: Material and State Conflict

This category evaluates inconsistencies in material or physical state:

“A melting ice sculpture in a snowy field.”  
“A steaming ice cube on a snowy ground.”  
“A wet fire burning with visible flames.”

Here:

$$g_{\text{state}}(x_0) \in \mathcal{S}_{\text{state}}(p),$$

which may violate typical thermodynamic or material consistency.

#### (8) DENS: Composition Density Variation

This category evaluates deviations in population or object density:

“A lightly crowded subway platform during peak hours.”  
“A lightly crowded shopping street during sales season.”  
“A lightly crowded bus stop during commute time.”

The constraint is:

$$g_{\text{dens}}(x_0) \leq \tau(p),$$

where  $\tau(p)$  specifies a low-density threshold rather than strict absence.

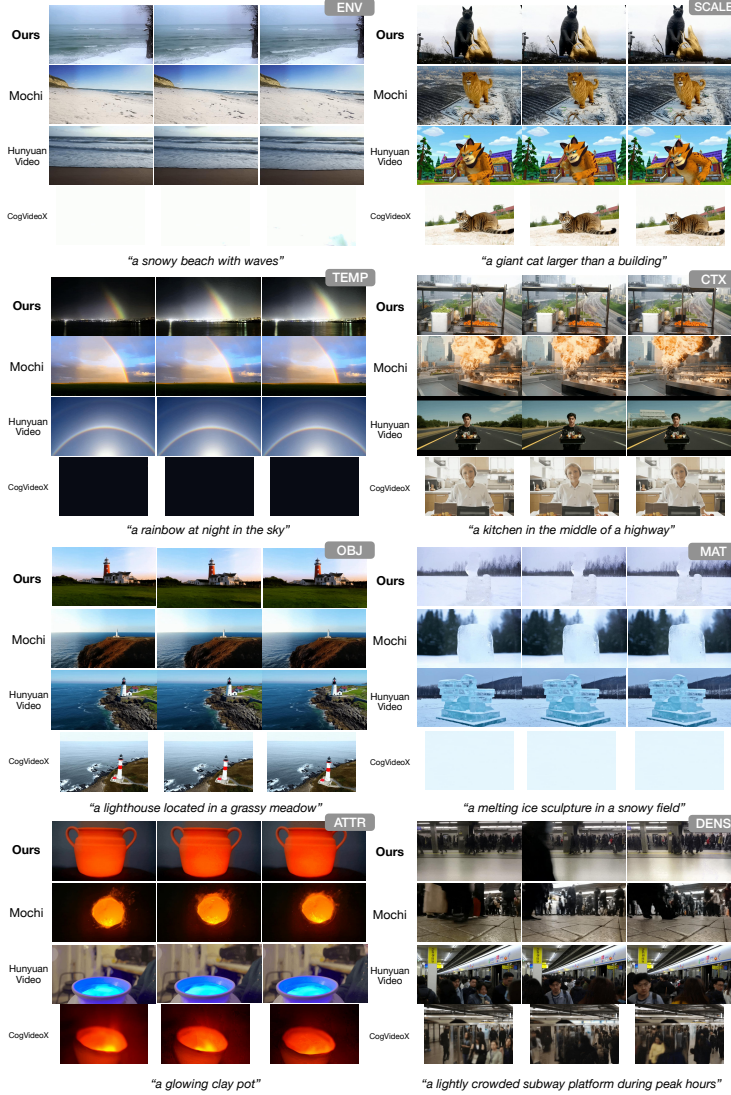


Figure 6: **Qualitative comparison across diverse compositional scenarios (Set 1).** We evaluate our method against state-of-the-art video diffusion models (Mochi, HunyuanVideo, CogVideoX) on eight rare compositional categories: ENV (Environment Recomposition), TEMP (Temporal Misalignment), OBJ (Object Relocation), ATTR (Attribute Rebinding), SCALE (Scale Shift), CTX (Contextual Relocation), MAT (Material and State Conflict), and DENS (Composition Density Variation). Each row shows frames sampled from generated videos for a representative prompt per category. Baseline models consistently collapse toward frequent semantic alternatives—for instance, generating a daytime rainbow instead of a nocturnal one, or a tropical beach instead of a snowy one—whereas our method faithfully realizes both compositional factors simultaneously, resisting default completion bias while preserving overall scene coherence.

**Summary.** Together, ENV, TEMP, OBJ, ATTR, SCALE, CTX, MAT, and DENS form a structured evaluation suite that probes multiple dimensions of compositional collapse, including environment recomposition, temporal misalignment, object-context mismatch, attribute binding, scale consistency, contextual placement, material-state coherence, and density variation.

Each category isolates a specific semantic factor  $g_k$ , enabling fine-grained analysis of failure modes in diffusion models. By explicitly modeling compositional constraints as in Eq. (18), the benchmark provides a principled framework for evaluating compositional fidelity in generative diffusion systems.

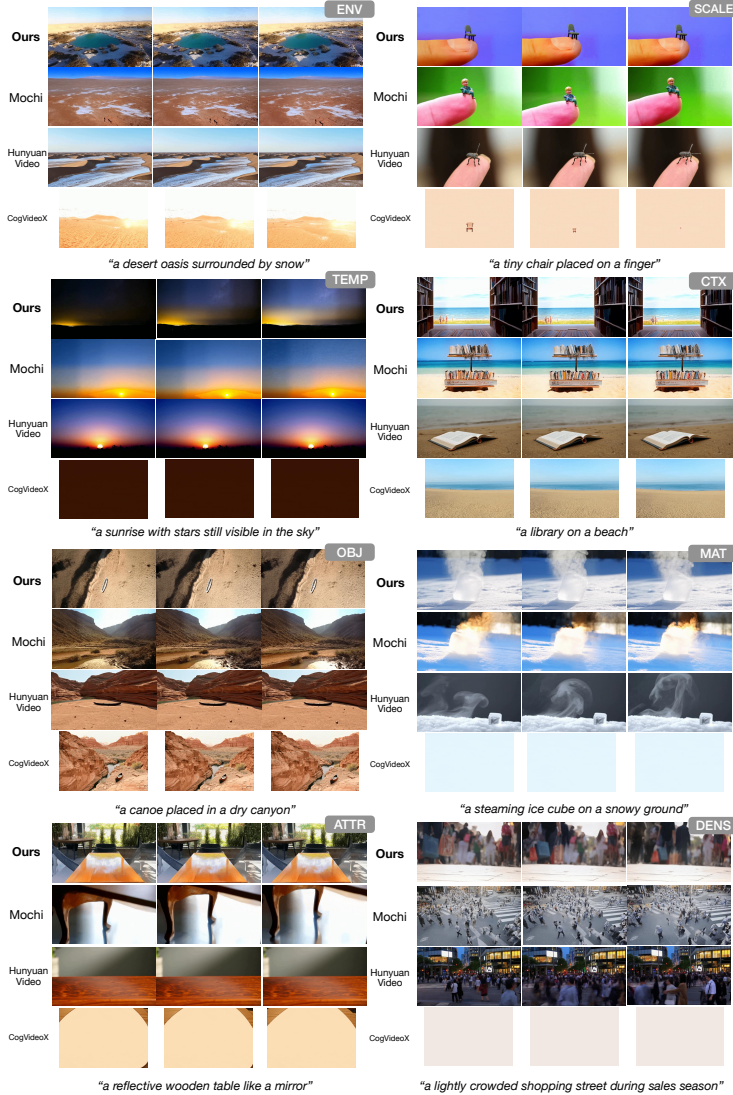


Figure 7: **Qualitative comparison across diverse compositional scenarios (Set 2)**. This figure presents a second set of representative prompts covering the same eight compositional categories as in Figure 6 (ENV, TEMP, OBJ, ATTR, SCALE, CTX, MAT, DENS). These examples include more challenging compositions such as *a desert oasis surrounded by snow*, *a tiny chair placed on a finger*, and *a steaming ice cube on snowy ground*. While baseline models frequently drift toward high-frequency alternatives or fail to realize the intended rare factor, our method consistently suppresses attractor-driven collapse and produces semantically coherent outputs across diverse scene contexts, from natural environments to structured indoor and object-level compositions.

## C Detailed Qualitative Results

Figures 6, 7, and 8 present qualitative comparisons across all eight compositional categories of DCR-Bench, spanning three sets of representative prompts. For each prompt, we show uniformly sampled frames from videos generated by Mochi, HunyuanVideo, CogVideoX, and our method (DCR applied to Mochi).

**ENV and TEMP.** Environment recomposition and temporal misalignment represent cases where the rare compositional factor directly conflicts with a dominant distributional prior. In ENV, baseline models consistently collapse toward a single-environment mode: for example, *a snowy beach with waves* is rendered as a standard tropical or sandy beach by all baselines, while our method preserves

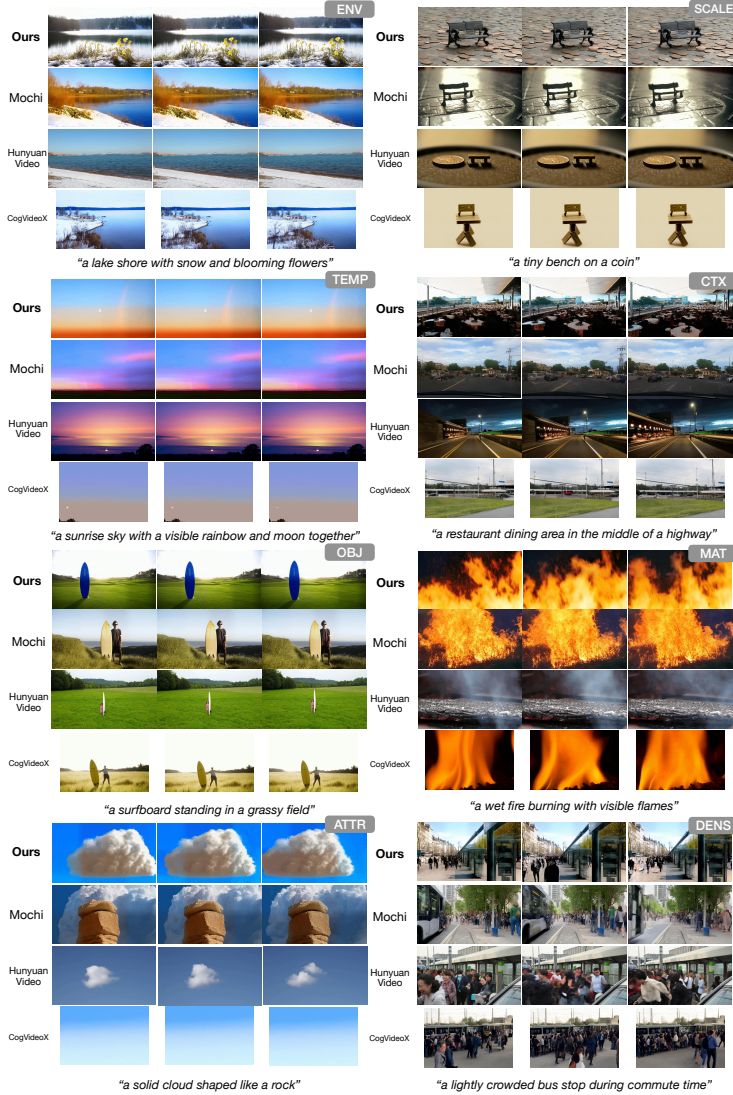


Figure 8: **Qualitative comparison across diverse compositional scenarios (Set 3).** This figure presents a third set of prompts spanning all eight compositional categories, including *a lake shore with snow and blooming flowers*, *a surfboard standing in a grassy field*, *a solid cloud shaped like a rock*, and *a wet fire burning with visible flames*. These cases probe more subtle compositional conflicts, such as simultaneous material-state inconsistency and attribute rebinding. Across all settings, baseline models exhibit attractor collapse toward more common scene configurations, whereas our method applies targeted repulsion to maintain the intended rare composition without degrading visual quality or scene realism.

both the beach setting and the snow simultaneously. In TEMP, cases such as *a rainbow at night in the sky* reveal a strong daytime prior in all backbone models—Mochi and HunyuanVideo generate brightly lit scenes with daytime rainbows, and CogVideoX produces a fully dark frame, failing to realize either factor. Our method generates a coherent nocturnal scene with a visible rainbow, successfully realizing both temporal and atmospheric components.

**OBJ and CTX.** Object relocation and contextual relocation probe whether models can place objects or scene elements in environments that deviate from typical co-occurrence patterns. In OBJ, prompts such as *a lighthouse located in a grassy meadow* and *a canoe placed in a dry canyon* require placing an object in an atypical environment. Baselines frequently revert the setting to the most common context for the object—placing the lighthouse on a rocky coast, or the canoe on a river. Our method

Method	CLIPScore $\uparrow$	CLIP-attr $\downarrow$	BLIP $\uparrow$	CCS $\uparrow$	CVR $\downarrow$
Mochi	0.3040 $\pm$ 0.0262	0.2718 $\pm$ 0.0395	0.7807 $\pm$ 0.0834	3.8375 $\pm$ 1.2865	0.4725 $\pm$ 0.4998
HunyuanVideo	0.3067 $\pm$ 0.0312	0.2725 $\pm$ 0.0368	0.7819 $\pm$ 0.0811	3.9750 $\pm$ 1.2662	0.3750 $\pm$ 0.4847
CogVideoX	0.2858 $\pm$ 0.0491	0.2644 $\pm$ 0.0454	0.7290 $\pm$ 0.1180	3.1925 $\pm$ 1.6830	0.5175 $\pm$ 0.5003
<b>Ours</b>	<b>0.3131 <math>\pm</math> 0.0271</b>	<b>0.2558 <math>\pm</math> 0.0349</b>	<b>0.8075 <math>\pm</math> 0.0592</b>	<b>4.1300 <math>\pm</math> 1.2931</b>	<b>0.3100 <math>\pm</math> 0.4630</b>
Negative Prompt	0.2735 $\pm$ 0.0363	0.2610 $\pm$ 0.0362	0.7065 $\pm$ 0.0813	3.0375 $\pm$ 1.5466	0.4375 $\pm$ 0.4966
Ours w/o Attractor Prompt	0.3088 $\pm$ 0.0327	0.2709 $\pm$ 0.0415	0.7794 $\pm$ 0.0849	3.9275 $\pm$ 1.3215	0.3400 $\pm$ 0.4743
Ours w/o Repulsion	0.3088 $\pm$ 0.0319	0.2732 $\pm$ 0.0402	0.7729 $\pm$ 0.0788	3.9500 $\pm$ 1.3006	0.3475 $\pm$ 0.4767
Ours w/o Schedule	0.3115 $\pm$ 0.0309	0.2740 $\pm$ 0.0402	0.7819 $\pm$ 0.0851	3.9675 $\pm$ 1.3155	0.3550 $\pm$ 0.4791

Table 2: **Quantitative evaluation results.** All metrics are reported as mean  $\pm$  standard deviation over the full evaluation set. Mochi, HunyuanVideo, and CogVideoX denote standard CFG baselines. Negative Prompt denotes the baseline where  $p_{\text{attr}}$  is provided as a negative prompt within standard CFG on Mochi. Ablation variants are based on Mochi. CCS denotes the Compositional Compliance Score and CVR denotes the Compositional Violation Rate, both obtained from a GPT-4o vision-language judge.

maintains the intended environment while correctly placing the object within it. In CTX, prompts such as *a kitchen in the middle of a highway* and *a restaurant dining area in the middle of a highway* are particularly challenging, as both contextual elements must be jointly realized. Baselines tend to generate either the kitchen or the highway in isolation, while our method produces coherent compositions that integrate both elements.

**ATTR and SCALE.** Attribute rebinding and scale shift test the model’s ability to assign unusual properties to objects. In ATTR, *a glowing clay pot* elicits strong responses: Mochi and CogVideoX produce glowing outputs, but with incorrect material renderings, while HunyuanVideo generates a completely different glowing object. Our method correctly combines the clay pot form with a luminous attribute. For SCALE, prompts such as *a giant cat larger than a building* and *a tiny bench on a coin* require scale relationships that are drastically different from learned priors. Baselines consistently generate objects at typical scales, ignoring the compositional constraint. Our method realizes the intended scale relationship, placing a miniature bench on a coin surface or rendering a cat at building scale with spatial coherence.

**MAT and DENS.** Material-state conflict and density variation represent the most subtle compositional challenges. In MAT, prompts such as *a melting ice sculpture in a snowy field* and *a wet fire burning with visible flames* require physically inconsistent but visually describable states. Mochi and HunyuanVideo tend to generate one state or the other—either a static ice sculpture or a standard fire—while our method produces outputs that incorporate both states. In DENS, prompts such as *a lightly crowded subway platform during peak hours* require the model to generate a scene that contradicts its density prior. Baselines produce crowded platforms consistent with typical peak-hour scenes, whereas our method generates a visibly sparse platform that nonetheless preserves the environmental context.

**Overall Observations.** Across all three sets, a consistent failure pattern emerges in baseline models: the denoising trajectory collapses toward the most statistically dominant completion, ignoring one or both compositional factors specified in the prompt. This manifests as environment substitution in ENV, temporal collapse in TEMP, context reversion in OBJ and CTX, attribute neglect in ATTR and SCALE, and state simplification in MAT. Our method applies targeted repulsion along the attractor direction at each denoising step, preventing this collapse while preserving the remaining semantic components of the guidance update. The results demonstrate that Default Completion Repulsion enables reliable generation of rare but semantically valid compositions that standard diffusion models consistently fail to produce.

## D Detailed Quantitative Evaluation

We evaluate whether generated videos satisfy the full compositional constraint using five complementary metrics. Our evaluation focuses on compositional fidelity: whether the generated video simultaneously realizes both constituent factors of the intended rare composition, and whether it resists collapse toward the more frequent attractor completion.

**CLIPScore.** We compute CLIPScore by measuring cosine similarity between each generated frame and the full textual prompt  $p$ . For a video consisting of  $T$  frames  $\{I_t\}_{t=1}^T$  and prompt  $p$ , we compute

$$\text{CLIPScore} = \frac{1}{T} \sum_{t=1}^T \cos(E_{\text{img}}(I_t), E_{\text{text}}(p)).$$

Higher CLIPScore indicates stronger global alignment between the generated video and the full intended composition.

**CLIP Similarity to Attractor Prompt (CLIP-attr).** To measure the degree of collapse toward the frequent counterpart, we compute the cosine similarity between generated frames and the attractor prompt  $p_{\text{attr}}$ :

$$\text{CLIP-attr} = \frac{1}{T} \sum_{t=1}^T \cos(E_{\text{img}}(I_t), E_{\text{text}}(p_{\text{attr}})).$$

Lower CLIP-attr values indicate stronger suppression of the default completion tendency. This metric is the DCR analogue of CLIP-neg used in negation-aware generation evaluation [22], adapted to measure attractor-directional collapse rather than forbidden concept presence. Because  $p_{\text{attr}}$  is explicitly defined as part of our framework, this metric directly reflects the core failure mode our method targets.

**BLIP Caption Alignment.** We evaluate semantic fidelity using BLIP-based captioning. For each frame, we generate a caption  $\hat{C}_t$  using a pretrained BLIP model and compute its similarity to the original prompt:

$$\text{BLIP} = \frac{1}{T} \sum_{t=1}^T \cos(E_{\text{text}}(\hat{C}_t), E_{\text{text}}(p)).$$

This provides a complementary text-level consistency measure based on generated descriptions rather than direct image-text matching. Unlike CLIPScore, which compares visual features against the prompt embedding directly, BLIP evaluates whether the semantic content of generated frames, as interpreted by an independent captioning model, is consistent with the intended composition.

Together, CLIPScore, CLIP-attr, and BLIP quantify (1) global prompt alignment, (2) attractor suppression, and (3) caption-level compositional fidelity, providing embedding-space measurements that are complementary in their sensitivity to different aspects of generation quality.

**Vision-Language Compositional Compliance Evaluation (CCS and CVR).** While the preceding metrics operate within embedding spaces, they do not directly verify whether both compositional factors are simultaneously present and coherently realized in the generated video. In particular, embedding-based metrics may fail to capture cases where one compositional factor dominates the visual representation while the other is absent, or where the generation reflects the attractor completion at a semantic level not fully captured by cosine similarity. To address this limitation, we introduce two complementary metrics based on a direct vision-language judge: the *Compositional Compliance Score (CCS)* and the *Compositional Violation Rate (CVR)*.

**Evaluation Principle.** Instead of comparing embeddings, we directly query a multimodal large language model capable of joint visual and textual reasoning. The judge receives (i) the full original textual prompt  $p$  describing the intended rare composition, (ii) the two constituent compositional factors extracted from  $p$  (e.g., *snowy* and *beach* for the prompt *a snowy beach*), (iii) the attractor prompt  $p_{\text{attr}}$  representing the frequent counterpart (e.g., *a tropical beach*), and (iv) multiple frames uniformly sampled from the generated video across its temporal span. The frames are resized with preserved aspect ratio to ensure consistent visual input resolution. No cropping, object masking, or post-processing is applied.

**Judge Configuration.** We use GPT-4o as a multimodal judge accessed through the OpenAI API. The model is instructed to evaluate *compositional fidelity only*, explicitly assessing whether both specified factors are simultaneously present and coherently composed in the video, and whether the output reflects the intended rare composition rather than the frequent attractor counterpart. The evaluation rubric is fixed and provided verbatim to the judge to ensure consistency across all evaluated samples. The model operates with deterministic decoding (temperature set to 0) to reduce stochastic variability.

**Scoring Rubric.** For each video, the judge assigns an integer score  $s \in \{1, 2, 3, 4, 5\}$  defined as:

- 1: Neither compositional factor is present; the output reflects neither the intended composition nor a semantically coherent alternative.
- 2: Only one compositional factor is present, or the output has collapsed entirely toward the attractor completion  $p_{\text{attr}}$ .
- 3: Both factors are partially present but incoherently composed, or the output is ambiguous between the intended composition and the attractor.
- 4: Both factors are present and mostly coherently composed, with minor ambiguity or imperfection.
- 5: Both factors are fully and coherently present; the output clearly reflects the intended rare composition rather than the frequent alternative.

In addition, the judge outputs a binary indicator `collapsed`, set to True when the generated video is judged to reflect the attractor prompt  $p_{\text{attr}}$  rather than the intended rare composition  $p$ , based on the judge’s multimodal reasoning over the provided frames.

**Compositional Compliance Score (CCS).** Let  $s_i$  denote the integer compliance score assigned to video  $i$  among  $N$  evaluated samples. We define:

$$\text{CCS} = \frac{1}{N} \sum_{i=1}^N s_i.$$

CCS ranges from 1 to 5. Higher values indicate stronger simultaneous realization of both compositional factors in the generated video.

**Compositional Violation Rate (CVR).** Let  $v_i$  be defined as:

$$v_i = \begin{cases} 1 & \text{if } \text{collapsed}_i = \text{True}, \\ 0 & \text{otherwise.} \end{cases}$$

We define:

$$\text{CVR} = \frac{1}{N} \sum_{i=1}^N v_i.$$

CVR measures the empirical frequency of attractor collapse across the evaluation set. Lower values indicate stronger resistance to default completion bias. CVR serves as the DCR analogue of the Negation Violation Rate (NVR) introduced in [22], adapted to measure collapse toward frequent compositional alternatives rather than presence of forbidden concepts.

**Aggregation Protocol.** All CCS and CVR values are computed over the full evaluation set without thresholding, sample exclusion, or post-hoc correction. Ambiguous cases (score = 3) are retained in the computation. The binary collapse indicator directly reflects the judge’s decision regarding attractor-directed generation, without manual reinterpretation.

**Rationale.** Unlike embedding-based metrics, CCS and CVR evaluate compositional fidelity through direct multimodal reasoning over visual evidence. This removes reliance on CLIP similarity space and avoids potential circularity arising from the fact that CLIP embeddings may not fully represent rare compositional semantics. By combining embedding-based alignment metrics with direct vision-language compliance scoring, we obtain complementary measurements of compositional fidelity and attractor suppression that operate at both the representational and reasoning levels.

**Overall Performance.** As summarized in Table 2, our method achieves the best performance across all evaluation metrics. In terms of embedding-based alignment, it improves CLIPScore (0.3131) over strong baselines such as HunyuanVideo (0.3067), while simultaneously reducing CLIP-attr (0.2558), indicating effective suppression of attractor bias without sacrificing global prompt alignment. Negative Prompt reduces CLIP-attr to 0.261, but at the cost of substantially lower CLIPScore (0.2735) and BLIP (0.7065), suggesting that naive attractor suppression via negative conditioning degrades overall semantic fidelity. In contrast, our method achieves lower CLIP-attr (0.2558)

Category	Method	CLIPScore $\uparrow$	CCS $\uparrow$	CVR $\downarrow$
ENV	Mochi	0.3010	3.5400	0.4800
	Negative Prompt	0.2777	3.3200	0.4000
	<b>Ours</b>	<b>0.3110</b>	<b>4.3600</b>	<b>0.3600</b>
TEMP	Mochi	0.3052	4.1400	0.4600
	Negative Prompt	0.2747	3.0400	0.4800
	<b>Ours</b>	<b>0.3061</b>	<b>4.2200</b>	<b>0.4000</b>
OBJ	Mochi	0.3310	3.8800	0.4200
	Negative Prompt	0.3076	3.9400	0.4200
	<b>Ours</b>	<b>0.3367</b>	<b>4.2400</b>	<b>0.2800</b>
ATTR	Mochi	0.2978	3.8200	0.5800
	Negative Prompt	0.2600	2.7600	0.4400
	<b>Ours</b>	<b>0.3065</b>	<b>3.8400</b>	<b>0.4000</b>
SCALE	Mochi	0.2996	3.8000	0.3600
	Negative Prompt	0.2782	3.5600	0.3000
	<b>Ours</b>	<b>0.3178</b>	<b>3.9600</b>	<b>0.2800</b>
CTX	Mochi	0.3106	4.1000	0.3200
	Negative Prompt	0.2743	2.1200	0.5400
	<b>Ours</b>	<b>0.3287</b>	<b>4.1800</b>	<b>0.2600</b>
MAT	Mochi	0.2996	3.3800	0.7200
	Negative Prompt	0.2736	2.7400	0.5400
	<b>Ours</b>	<b>0.3061</b>	<b>4.1400</b>	<b>0.1800</b>
DENS	Mochi	0.2939	4.0400	0.4400
	Negative Prompt	0.2426	2.8200	0.3800
	<b>Ours</b>	<b>0.2932</b>	<b>4.1000</b>	<b>0.3200</b>

Table 3: **Category-wise quantitative evaluation on DCR-Bench.** We report CLIPScore ( $\uparrow$ ), CCS ( $\uparrow$ ), and CVR ( $\downarrow$ ) across all eight compositional categories. All methods use Mochi as the backbone unless otherwise noted. Categories are defined in Appendix B.

while simultaneously improving CLIPScore and BLIP (0.8075), demonstrating that projection-based repulsion avoids this trade-off. Our method also attains the highest BLIP score (0.8075), confirming improved semantic consistency at the caption level. More importantly, gains are even more pronounced in reasoning-based metrics. Our approach achieves the highest CCS (4.1300) and the lowest CVR (0.3100), substantially reducing attractor-driven collapse compared to Mochi (CVR: 0.4725) and Negative Prompt (CVR: 0.4375). This demonstrates that improvements are not limited to embedding similarity, but translate to actual compositional correctness under multimodal reasoning. Ablation results further validate the contribution of each component. Removing the attractor prompt leads to the largest performance drop, with CCS falling to 3.9275 and CVR increasing to 0.3400, indicating that explicit attractor modeling is the most critical component. Removing repulsion degrades CCS to 3.9500 and raises CVR to 0.3475, confirming that trajectory-level correction is necessary beyond probe computation alone. Removing the schedule further reduces CCS to 3.9675 and increases CVR to 0.3550, demonstrating that restricting repulsion to a targeted interval prevents over-correction of the denoising trajectory. Together, these results confirm that all three components contribute meaningfully to suppressing default completion bias and improving compositional fidelity.

**Category-wise Compositional Analysis.** Table 3 reports CLIPScore, CCS, and CVR across all eight compositional categories. Several consistent trends emerge from this breakdown. First, the benefits of DCR are most pronounced in categories that require suppression of strong distributional priors. In MAT, our method reduces CVR from 0.72 (Mochi) to 0.18, the largest absolute reduction across all categories, while improving CCS from 3.38 to 4.14. This indicates that material-state conflicts—such as *a melting ice sculpture in a snowy field*—are particularly susceptible to attractor collapse, and that targeted repulsion is highly effective in these settings. Similarly, in ENV, CVR drops from 0.48 to 0.36 with a CCS gain of +0.82, confirming that environment recomposition benefits strongly from explicit attractor suppression. Second, CTX and OBJ show the largest CLIPScore improvements (+0.018 and +0.006 respectively), alongside substantial CVR reductions. In CTX,

Negative Prompt produces the lowest CCS (2.12) among all methods and categories, confirming that naive negative conditioning is particularly harmful when both contextual elements must be jointly realized. Third, TEMP and CTX represent cases where Mochi itself achieves relatively high CCS (4.14 and 4.10), yet DCR still improves both CCS and CVR. This indicates that even when baseline models partially succeed, the attractor direction remains active and DCR provides meaningful additional suppression. Finally, DENS shows the smallest absolute CVR improvement ( $0.44 \rightarrow 0.32$ ), consistent with the observation that density constraints are more diffuse and harder to localize within the guidance update direction. Nevertheless, our method maintains Ours as the best-performing variant across all eight categories on all three reported metrics, confirming the broad applicability of the DCR framework.

**Rationale for Automated Evaluation.** Unlike embedding-based metrics that operate within CLIP feature space, CCS and CVR are obtained from GPT-4o, a multimodal model that directly reasons over video frames and assesses whether both compositional factors are simultaneously present and coherently realized—the same judgment a human annotator would perform. The judge is configured with a fixed rubric, deterministic decoding (temperature = 0), and explicit instructions to evaluate compositional fidelity only, minimizing subjectivity and ensuring consistency across all 400 evaluated samples. The validity of this protocol is supported by prior work on compositional video generation [22], which demonstrated that GPT-based compliance scoring and human perceptual evaluation yield consistent rankings across methods on closely related tasks, confirming that vision-language judge scores serve as a reliable proxy for human judgment of compositional fidelity.

## E Detailed Ablation Study

We provide extended quantitative and qualitative analysis of the four ablation variants reported in the main paper. Results are summarized in Table 2 and illustrated in Figure 4.

**Negative Prompt Baseline.** Providing  $p_{\text{attr}}$  as a CFG negative prompt constitutes the most direct alternative to our method, yet yields the worst overall performance. CLIPScore drops to  $0.2735 \pm 0.0363$  and BLIP to  $0.7065 \pm 0.0813$ , the lowest among all variants, while CCS falls to  $3.0375 \pm 1.5466$  and CVR remains elevated at  $0.4375 \pm 0.4966$ . Qualitatively, the generated frames are near-black and featureless, failing to render any compositional content. This failure arises because standard CFG negative guidance exerts an unconditional, undirected push away from  $p_{\text{attr}}$  at every denoising step, suppressing not only the unwanted attribute but the broader semantic context necessary to synthesize the rare composition. The results confirm that naive negation via CFG is fundamentally unsuitable for compositional rarity control.

**Effect of Removing the Attractor Prompt.** Without a semantically distinct  $p_{\text{attr}}$ , the probe branch collapses onto the main guidance direction, reducing the method to a guidance-scale relaxation baseline. CLIP-attr rises from 0.2558 to 0.2709 and CVR increases from 0.3100 to 0.3400, while CLIPScore and BLIP also degrade modestly. Qualitatively, the model reverts to a prototypical daytime sky scene, generating a visually coherent but semantically incorrect output that ignores the nocturnal context entirely. This confirms that the drift direction  $a_t$  carries no meaningful signal when the probe and target branches share the same conditioning: without a distinct  $p_{\text{attr}}$ , the repulsion mechanism has no well-defined direction to suppress, and compositional compliance deteriorates accordingly.

**Effect of Removing the Repulsion Update.** Retaining the attractor probe but setting  $\lambda_t = 0$  disables the projection-based correction while leaving all other components intact. This yields the largest increase in CLIP-attr among the ablation variants ( $0.2732 \pm 0.0402$ ), and CVR rises to  $0.3475 \pm 0.4767$ , with CCS falling to  $3.9500 \pm 1.3006$ . Qualitatively, the output drifts toward the model’s high-probability prior—a brightly lit daytime rainbow—despite the attractor branch correctly identifying the drift direction. CLIPScore is essentially unchanged (0.3088), confirming that global semantic conditioning is preserved but compositional suppression fails entirely. These results establish that computing the drift direction is necessary but insufficient: the corrective repulsion update is the operative mechanism that translates the identified bias into an effective guidance correction.

**Effect of Removing Constraint Scheduling.** Fixing  $\alpha_t = 1$  uniformly applies repulsion throughout the entire denoising trajectory, including early high-noise steps where global scene layout is determined. This produces the highest CVR among the three model-based ablations ( $0.3550 \pm 0.4791$ ) and the largest CLIP-attr ( $0.2740 \pm 0.0402$ ), despite a CLIPScore comparable to the full model (0.3115). Qualitatively, early-step interference disrupts coarse structure formation, yielding an oversaturated close-up arc that loses the intended nocturnal scene scale and context. The elevated CVR variance further indicates that suppression becomes unstable across prompts when the scheduling window is removed. These results confirm that temporally restricting repulsion to a targeted interval is essential: premature enforcement corrupts the structural scaffold before semantic detail can be reliably steered.

## F Attractor Trajectory Visualization

To validate that the attractor prompt  $p_{\text{attr}}$  accurately captures the model’s default completion tendency, we compare three generation conditions for each prompt: our full method (DCR), the Mochi baseline (standard CFG on prompt  $p$ ), and  $p_{\text{attr}}$  only (standard CFG on the attractor prompt alone, without repulsion). If  $p_{\text{attr}}$  correctly represents the model’s implicit attractor, then the  $p_{\text{attr}}$ -only output should closely resemble the Mochi baseline output—both reflecting the frequent completion that DCR is designed to suppress. Figure 9 presents this comparison across three compositional categories. In ENV (*a snowy beach with waves*), both Mochi and the  $p_{\text{attr}}$ -only condition generate a snow-free sunny beach, while DCR produces a beach with visible snow and waves. In TEMP (*a rainbow at night in the sky*), Mochi generates a daytime or twilight rainbow, and the  $p_{\text{attr}}$ -only condition produces a similar warm-toned twilight scene, whereas DCR generates a coherent nocturnal scene with a visible rainbow. In ATTR (*a glowing clay pot*), Mochi collapses to a glowing spherical object, while the  $p_{\text{attr}}$ -only condition produces a clay pot under dimmer lighting, closer to the intended relaxed completion. DCR correctly realizes the glowing attribute while preserving the clay pot form. Across all three categories, the  $p_{\text{attr}}$ -only outputs consistently reflect the model’s high-frequency completion preference and closely resemble the Mochi baseline, confirming that  $p_{\text{attr}}$  serves as an accurate proxy for the implicit attractor. This validates the core motivation of DCR: by explicitly modeling the attractor direction through  $p_{\text{attr}}$ , the method can apply targeted repulsion to prevent compositional collapse without degrading overall generation quality.

## G Attractor Prompt Generation Details

For each target prompt  $p$ , we generate the attractor prompt  $p_{\text{attr}}$  using a large language model (GPT-4o) via a structured rewriting instruction. The transformation is designed to remove or weaken the rare compositional factor while preserving the surrounding semantic context, producing a prompt that reflects the model’s most probable default completion.

**Prompting Template.** We use the following fixed instruction template:

```
Given the following text prompt describing a rare but
plausible visual composition, generate a single alternative
prompt that represents the most common or frequently occurring
version of the same scene. Remove or replace only the rare
compositional factor (e.g., unusual attribute, atypical
environment, or unlikely object placement) while preserving
all other scene elements. Output only the rewritten prompt,
with no explanation.

Input prompt: {p}
```

All attractor prompts are generated with temperature set to 0 for deterministic output. Manual review is conducted to verify that each  $p_{\text{attr}}$  (i) removes the rare factor, (ii) preserves surrounding scene semantics, and (iii) does not introduce new compositional elements absent from the original prompt.

**Examples.** Table 4 lists representative  $(p, p_{\text{attr}})$  pairs across all eight benchmark categories.

Category	Prompt $p$	Attractor $p_{\text{attr}}$
ENV	a snowy beach with waves	a tropical beach with waves
ENV	a desert oasis surrounded by snow	a desert oasis surrounded by sand dunes
TEMP	a rainbow at night in the sky	a rainbow during the day in the sky
TEMP	a sunrise with stars still visible in the sky	a clear sunrise sky
OBJ	a lighthouse located in a grassy meadow	a lighthouse on a rocky coast
OBJ	a canoe placed in a dry canyon	a canoe on a calm river
ATTR	a glowing clay pot	a clay pot under natural lighting
ATTR	a reflective wooden table like a mirror	a wooden table under natural lighting
SCALE	a giant cat larger than a building	a cat near a building
SCALE	a tiny bench on a coin	a bench on the ground
CTX	a kitchen in the middle of a highway	a kitchen inside a house
CTX	a library on a beach	a library inside a building
MAT	a melting ice sculpture in a snowy field	an ice sculpture in a snowy field
MAT	a wet fire burning with visible flames	a fire burning with visible flames
DENS	a lightly crowded subway platform during peak hours	a crowded subway platform during peak hours
DENS	a lightly crowded shopping street during sales season	a busy shopping street during sales season

Table 4: **Representative**  $(p, p_{\text{attr}})$  **pairs across all eight benchmark categories.** Each attractor prompt removes or replaces the rare compositional factor while preserving the surrounding scene context.

## H Backbone Choice and Method Generality

**Scope.** The scientific contribution of this paper is the identification of *default completion bias* as a generative failure mode and the introduction of a projection-based repulsion mechanism that suppresses it at inference time. Establishing this contribution requires (i) demonstrating that the failure mode exists in modern text-to-video diffusion models and (ii) demonstrating that projection-based repulsion suppresses it in a controlled setting where each component of the method can be cleanly isolated. We address (i) across three backbones and (ii) on Mochi as a controlled testbed. Cross-backbone *calibration* of repulsion hyperparameters is a complementary engineering question and is discussed as future work.

**The target failure mode is empirically backbone-agnostic.** A central premise of DCR is that compositional collapse is not a quirk of any single model but a structural tendency of large-scale text-to-video diffusion systems. This is supported empirically by Section 4.3 and Appendix C: across all eight categories of DCR-Bench, Mochi, HunyuanVideo, and CogVideoX exhibit consistent collapse toward statistically dominant completions—daytime rainbows instead of nocturnal ones, snow-free beaches instead of snowy ones, glowing spheres instead of glowing clay pots. These three backbones differ in architecture (DiT-based vs. transformer-based), text encoder (T5 vs. LLM-based), scheduler family (flow-matching vs. v-prediction), and training data. The fact that all three exhibit the same failure pattern establishes that default completion bias is a property of the model *class* rather than of any specific backbone. The need for an explicit suppression mechanism is therefore established at the level of the class.

**DCR’s formulation is backbone-invariant by construction.** Given any diffusion model that supports classifier-free guidance with free-form text conditioning, DCR is fully specified by three operations: (i) three denoiser forward passes on the existing model, conditioned respectively on  $\emptyset$ ,  $p$ , and  $p_{\text{attr}}$ , requiring no modification to the transformer, scheduler, or text encoder; (ii) two linear combinations in noise-prediction space,  $\Delta_{\text{ref}} = w(\epsilon_{\text{text}} - \epsilon_{\text{uncond}})$  and  $\epsilon_{\text{probe}} = \epsilon_{\text{uncond}} + w_{\text{attr}}(\epsilon_{\text{attr}} - \epsilon_{\text{uncond}})$ ; and (iii) one projection  $\Delta_t^* = \Delta_{\text{ref}} - \lambda_t a_t$ , computed via an inner product and a norm over flattened latent tensors. None of these operations references the architecture, the scheduler family, the parameterization (noise-prediction vs. flow), or the text encoder of the underlying model. The formulation is therefore backbone-invariant in the same sense that classifier-free guidance [18] itself is.

**What varies across backbones is calibration, not mechanism.** The only quantity DCR inherits from each backbone is the *magnitude scale* of  $\epsilon_{\text{text}} - \epsilon_{\text{uncond}}$ , which determines appropriate values of  $(w, w_{\text{attr}}, \eta)$ . Different backbones already use different default guidance scales for this reason, independently of DCR. Calibrating these hyperparameters per backbone is therefore a per-backbone hyperparameter exercise of the same kind that any guidance-based method inherits, not a test of whether the repulsion mechanism itself generalizes. Section 4.7 (Hyperparameter Sensitivity) shows that DCR is robust within a broad range of these values on Mochi, suggesting that calibration overhead on new backbones is modest rather than load-bearing.

**Why Mochi specifically.** Within this scope, we select Mochi as the primary testbed for three reasons. First, it exposes a clean classifier-free guidance interface through the standard `diffusers` library, allowing the three-branch forward pass to be implemented without modifying any internal component. Second, its T5-based conditioning and flow-matching scheduler represent a widely adopted configuration in recent open-source text-to-video systems, making it a representative rather than idiosyncratic choice. Third, its publicly available, self-contained inference pipeline ensures that all experiments are fully reproducible without proprietary components. These properties make Mochi a controlled environment for isolating the effect of the proposed mechanism via the ablations in Table 1.

**Future work.** A systematic multi-backbone quantitative study—including HunyuanVideo, CogVideoX, and image-domain backbones such as SDXL and SD3—would require per-backbone calibration of  $(w, w_{\text{attr}}, \eta, r_s, r_e)$  alongside backbone-specific evaluation protocols. We view this as a natural and important extension that builds on the mechanism established here, and leave it to future work.

## I Computation Time and Memory Consumption

Model	Step	Memory Consumption	Computation Time
Ours	Inference	26.3096 GB / 80.0000 GB (26,941 MiB)	192 sec
Ours w/o Attractor Prompt	Inference	25.0264 GB / 80.0000 GB (25,627 MiB)	190 sec
Ours w/o Repulsion	Inference	25.4287 GB / 80.0000 GB (26,039 MiB)	176 sec
Ours w/o Schedule	Inference	25.0264 GB / 80.0000 GB (25,627 MiB)	187 sec
Negative Prompt	Inference	28.2496 GB / 80.0000 GB (26,941 MiB)	174 sec
Mochi	Inference	26.2406 GB / 80.0000 GB (25,025 MiB)	114 sec
HunyuanVideo	Inference	41.3589 GB / 80.0000 GB (39,443 MiB)	396 sec
CogVideoX	Inference	16.7845 GB / 80.0000 GB (16,007 MiB)	61 sec

Table 5: **Inference-time memory and runtime on a single NVIDIA H100 (80GB).** Peak GPU memory and end-to-end inference time are reported for our full method, ablation variants, and all baselines. All methods share the same backbone (Mochi) except HunyuanVideo and CogVideoX. All measurements are conducted under identical hardware and evaluation conditions.

Table 5 reports peak GPU memory and end-to-end inference time on a single NVIDIA H100 (80GB) for all evaluated methods.

**Computational overhead of DCR.** Our full method requires three denoiser forward passes per step: unconditional, text-conditioned, and attractor-conditioned. Compared to Mochi (standard two-branch CFG, 114 sec), DCR adds approximately 78 sec (+68%), reflecting the cost of the additional attractor branch forward pass. Peak memory increases marginally from 26.24 GB (Mochi) to 26.31 GB (Ours), as the three branches share the same model weights and the additional activation footprint is modest. The projection-based repulsion contributes negligible overhead beyond the forward pass, as it requires only a scalar inner-product and norm computation over flattened latent tensors.

**Ablation variants.** Removing the attractor prompt reduces the method to two-branch CFG with a redundant projection (190 sec, 25.03 GB), nearly matching the runtime of the full model since the forward-pass count remains the same. Removing repulsion (176 sec, 25.43 GB) yields a modest speedup by skipping the projection correction at each step. Removing the schedule (187 sec, 25.03

GB) applies repulsion uniformly across all steps; runtime is comparable to the full model since the active interval  $[r_s, r_e] = [0.2, 0.8]$  already covers the majority of denoising steps.

**Comparison across backbones.** Negative Prompt uses the same three-branch structure as DCR but applies the attractor branch as a standard CFG negative input, resulting in 174 sec and 28.25 GB. Among the backbone baselines, HunyuanVideo requires the most resources at 41.36 GB and 396 sec, while CogVideoX is the most efficient at 16.78 GB and 61 sec. Our method’s overhead relative to Mochi is modest and represents a practical trade-off for improved compositional fidelity.

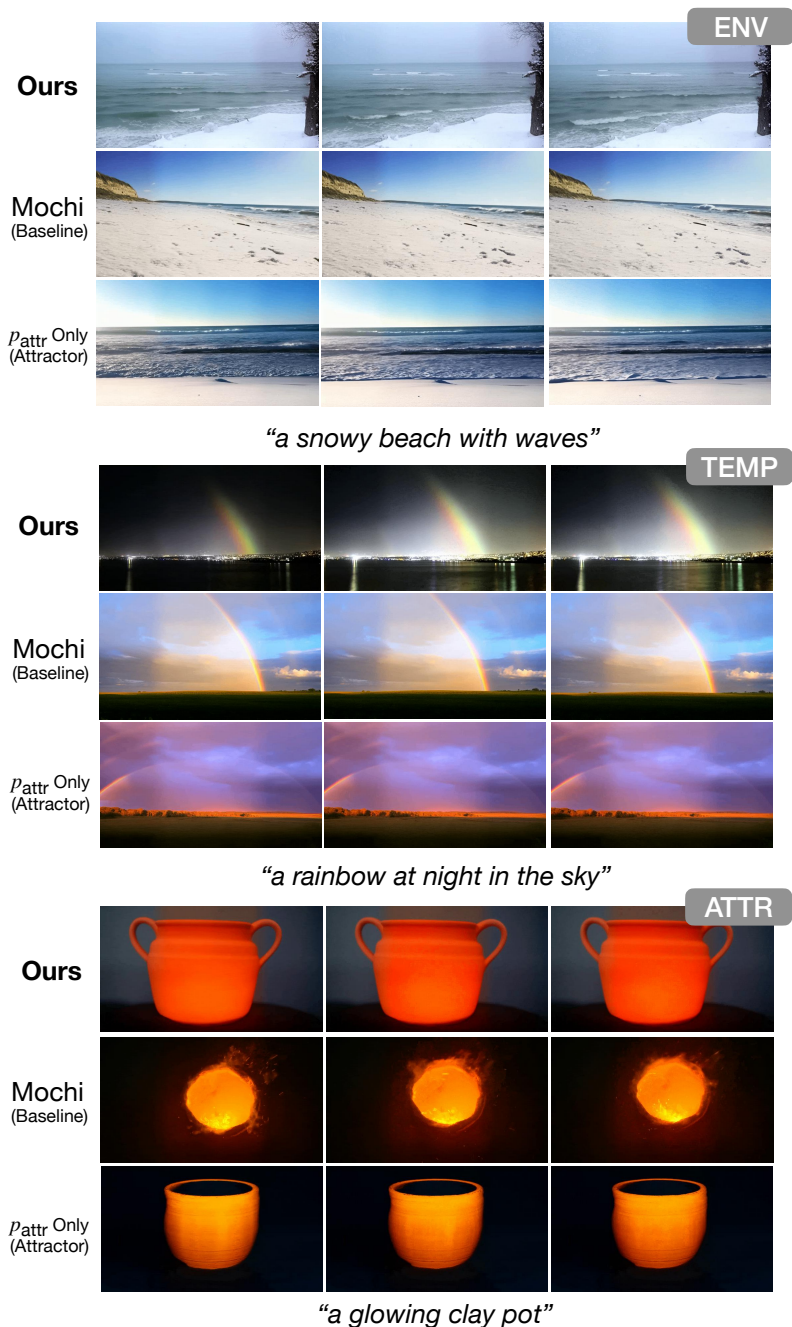


Figure 9: **Attractor trajectory visualization across three compositional categories.** For each prompt, we compare videos generated by Ours (DCR), Mochi (standard CFG baseline), and  $p_{\text{attr}}$  only (standard CFG applied to the attractor prompt). In all three cases, the  $p_{\text{attr}}$ -only output reflects the model’s default completion tendency—a sunny beach instead of a snowy one (ENV), a daytime rainbow instead of a nocturnal one (TEMP), and a dimly lit clay pot instead of a glowing one (ATTR)—and closely resembles the Mochi baseline output. This confirms that  $p_{\text{attr}}$  serves as an accurate proxy for the model’s implicit attractor, and that DCR effectively suppresses this tendency to generate rare but semantically valid compositions.



Figure 10: **ENV (Environment Recomposition)**. Prompt: “a snowy beach with waves.” Our method preserves both snow and beach simultaneously, while baselines collapse to a standard beach.



Figure 11: **TEMP (Temporal Misalignment)**. Prompt: “a rainbow at night in the sky.” Our method generates a nocturnal rainbow, whereas baselines revert to daytime scenes.



Figure 12: **OBJ (Object Relocation)**. Prompt: “a lighthouse located in a grassy meadow.” Our method maintains the rare object-environment pairing, while baselines relocate the object to coastal regions.

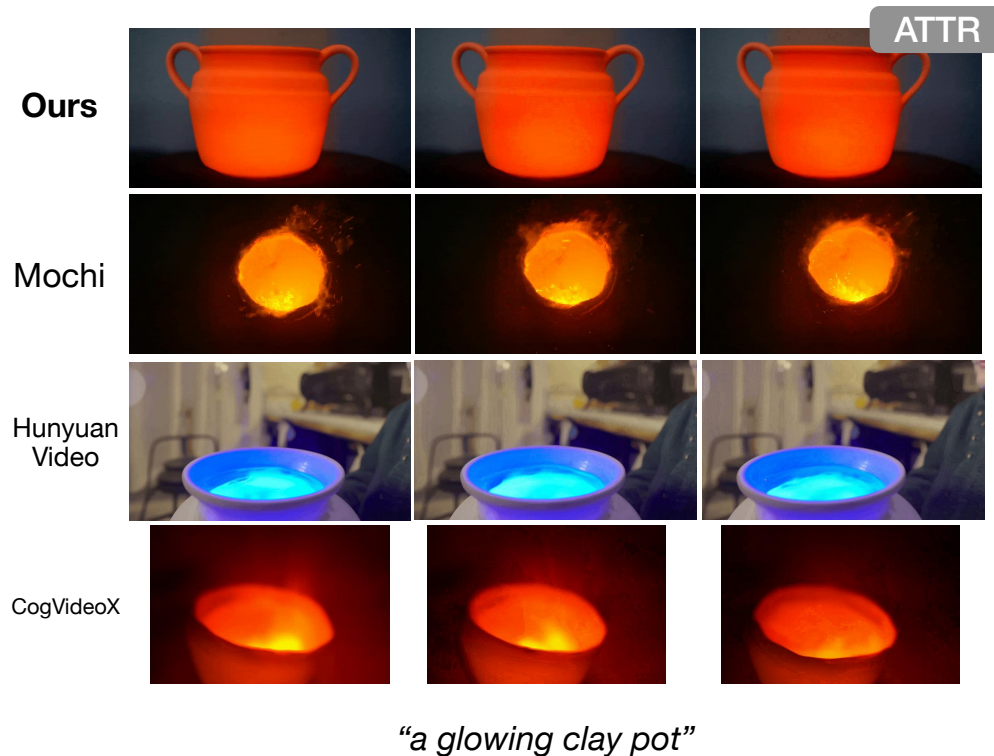


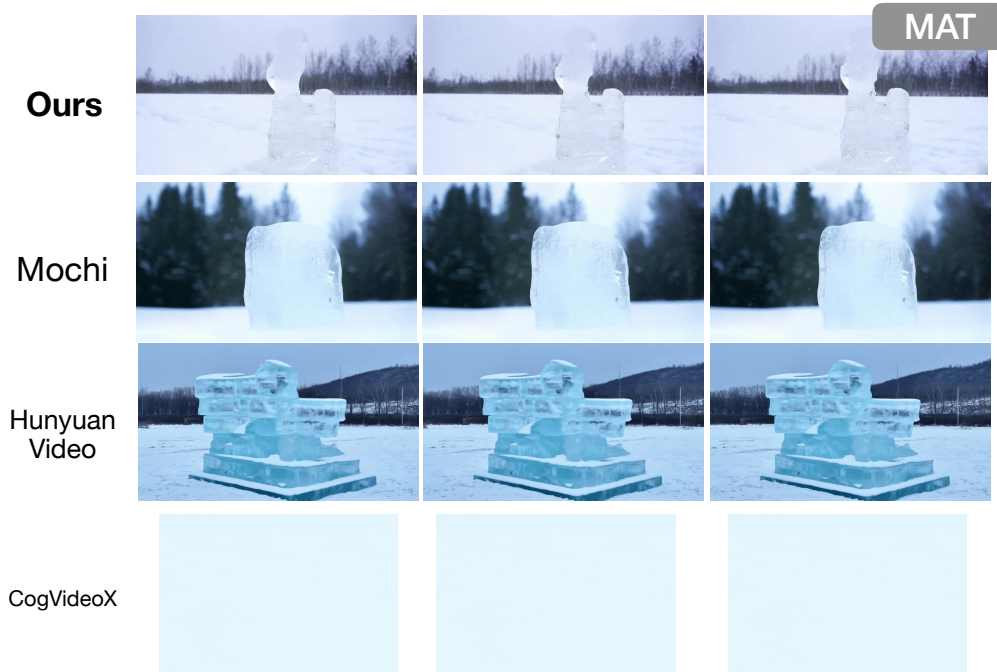
Figure 13: **ATTR (Attribute Rebinding)**. Prompt: “a glowing clay pot.” Our method correctly binds the glowing attribute to the clay material, while baselines alter object identity or material.



Figure 14: **SCALE (Scale Shift)**. Prompt: “a giant cat larger than a building.” Our method realizes extreme scale relationships, while baselines revert to typical object sizes.

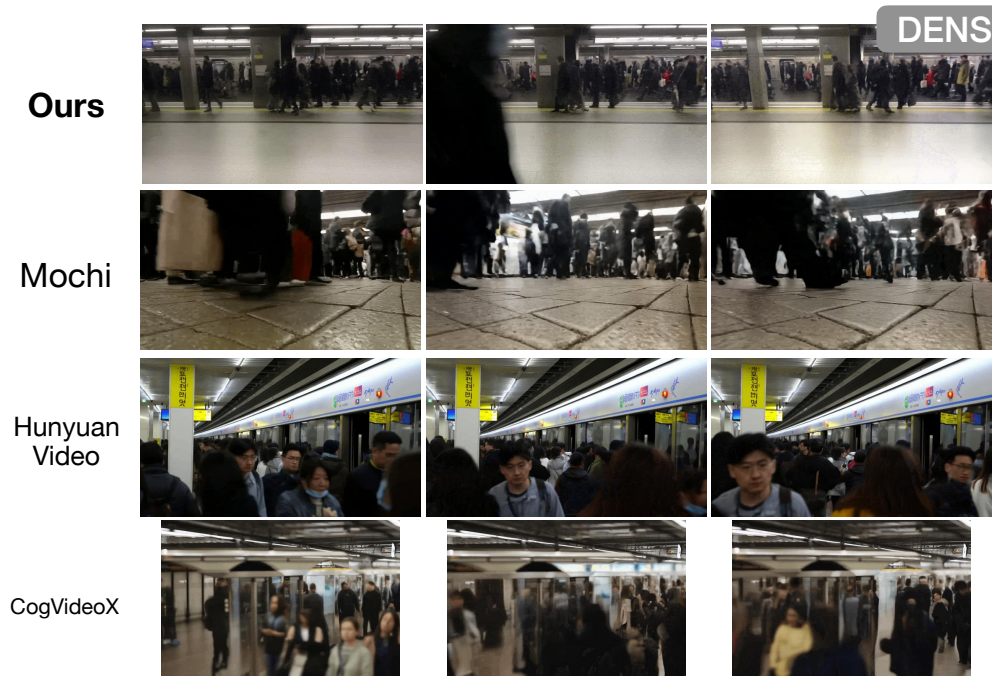


Figure 15: **CTX (Contextual Relocation)**. Prompt: “a kitchen in the middle of a highway.” Our method integrates both contexts coherently, while baselines generate only one dominant scene.



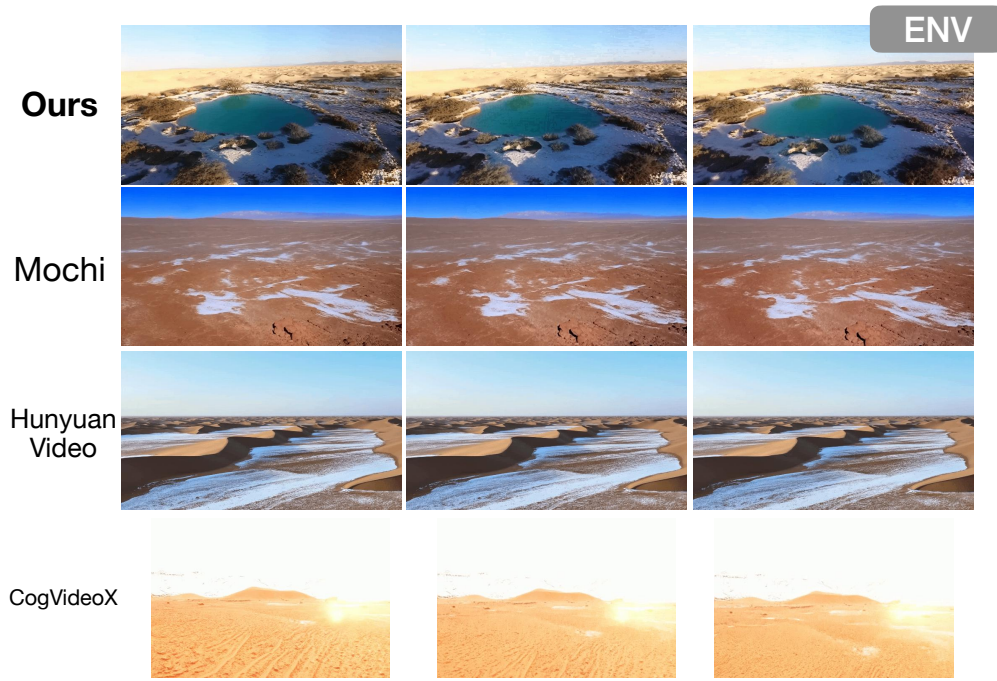
*“a melting ice sculpture in a snowy field”*

Figure 16: **MAT (Material-State Conflict)**. Prompt: “a melting ice sculpture in a snowy field.” Our method preserves both melting and snowy conditions, while baselines collapse to a single state.



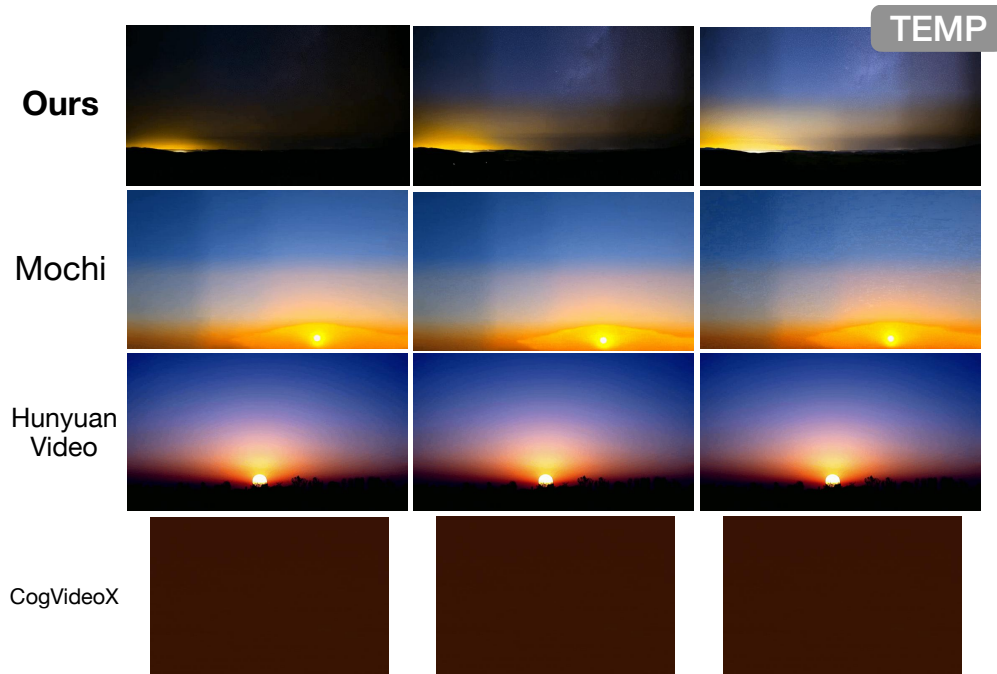
*“a lightly crowded subway platform during peak hours”*

Figure 17: **DENS (Density Variation)**. Prompt: “a lightly crowded subway platform during peak hours.” Our method maintains low density despite strong priors for crowded scenes.



*“a desert oasis surrounded by snow”*

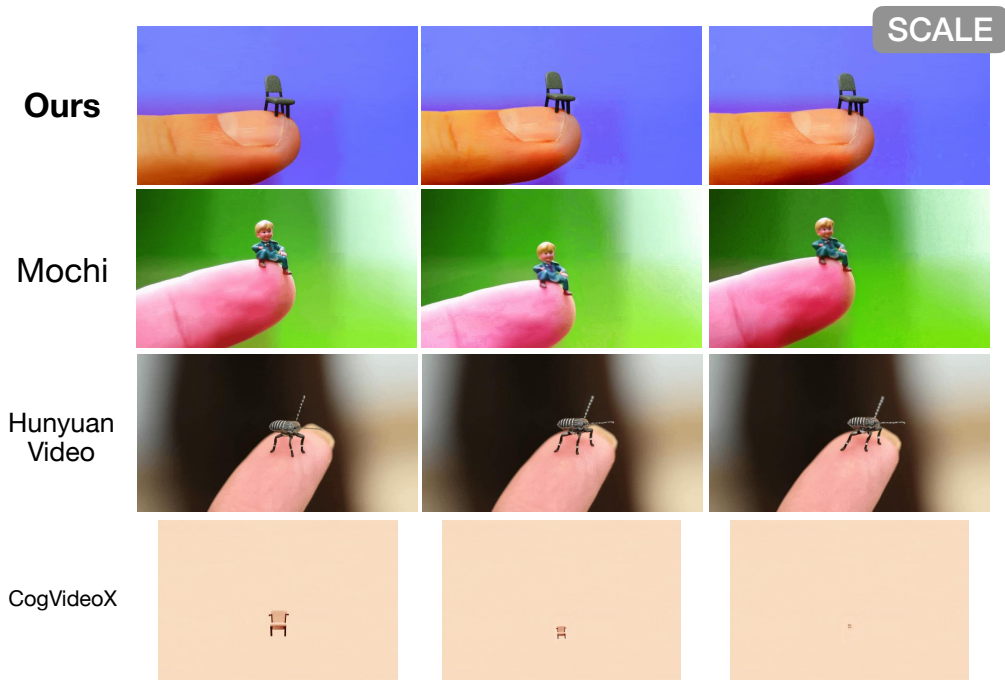
Figure 18: **ENV**. Prompt: “a desert oasis surrounded by snow.”



*“a sunrise with stars still visible in the sky”*

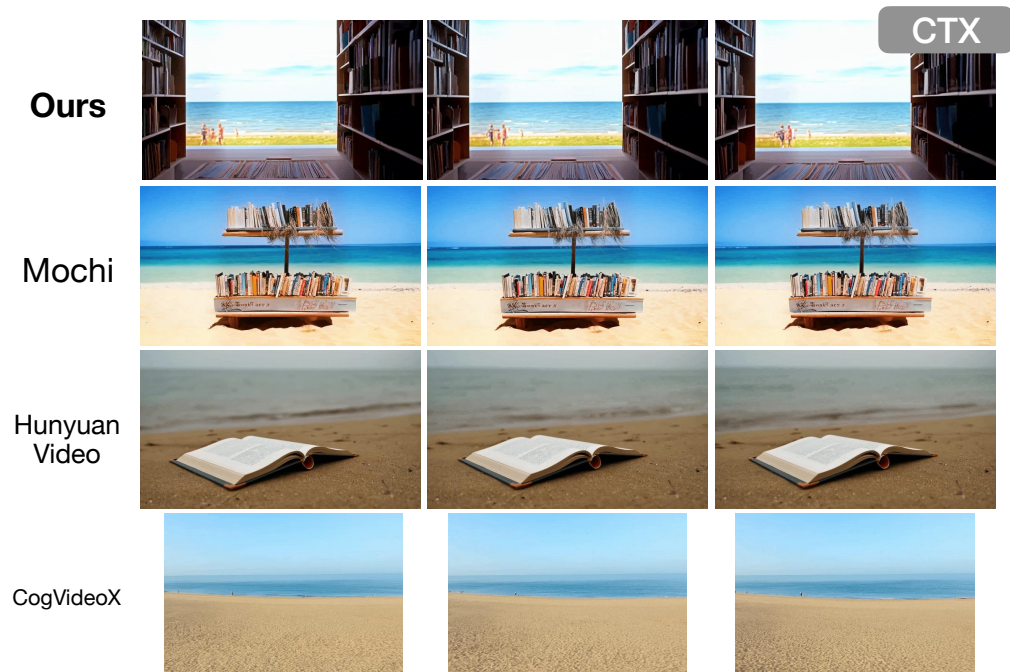
Figure 19: **TEMP**. Prompt: “a sunrise with stars still visible in the sky.”





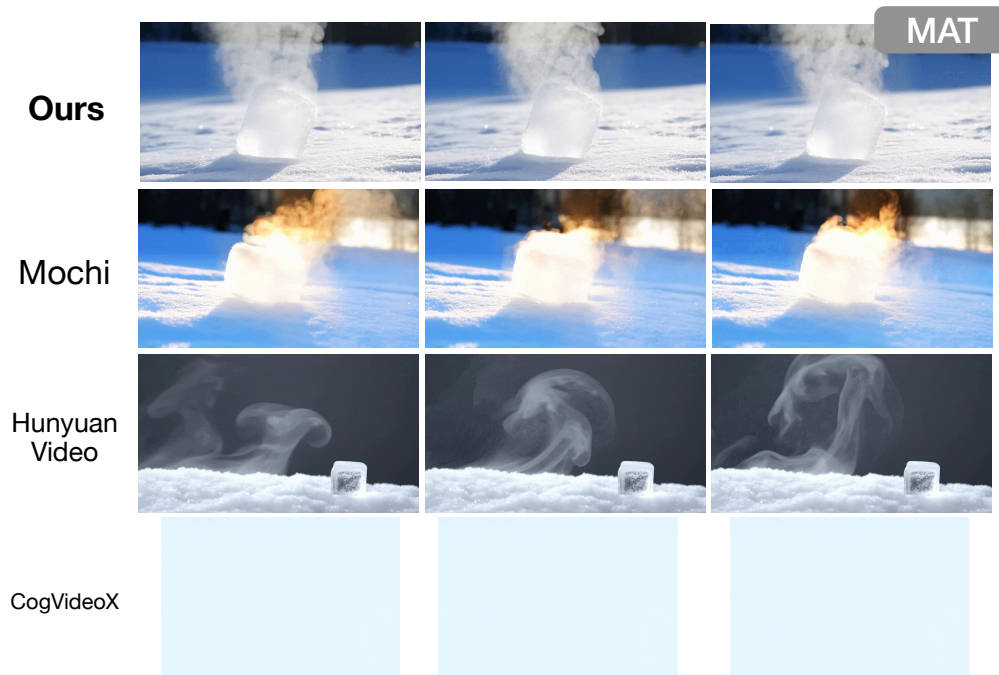
*“a tiny chair placed on a finger”*

Figure 22: **SCALE**. Prompt: “a tiny chair placed on a finger.”



*“a library on a beach”*

Figure 23: **CTX**. Prompt: “a library on a beach.”



*“a steaming ice cube on a snowy ground”*

Figure 24: **MAT**. Prompt: “a steaming ice cube on a snowy ground.”



*“a lightly crowded shopping street during sales season”*

Figure 25: **DENS**. Prompt: “a lightly crowded shopping street during sales season.”



Figure 26: **ENV.** Prompt: “a lake shore with snow and blooming flowers.”

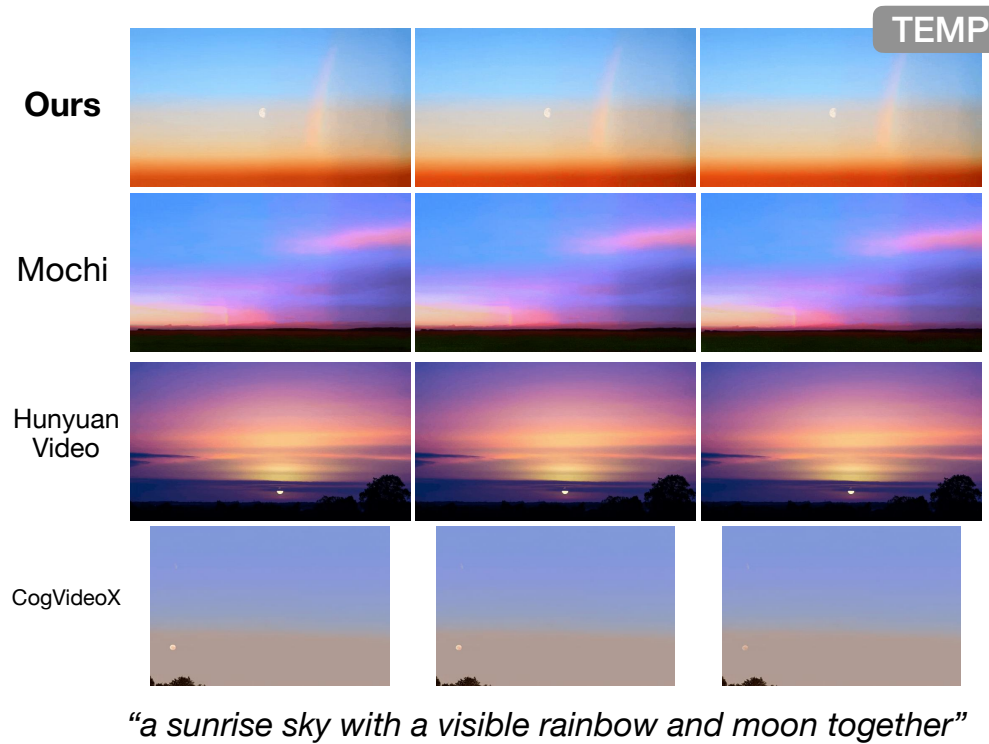
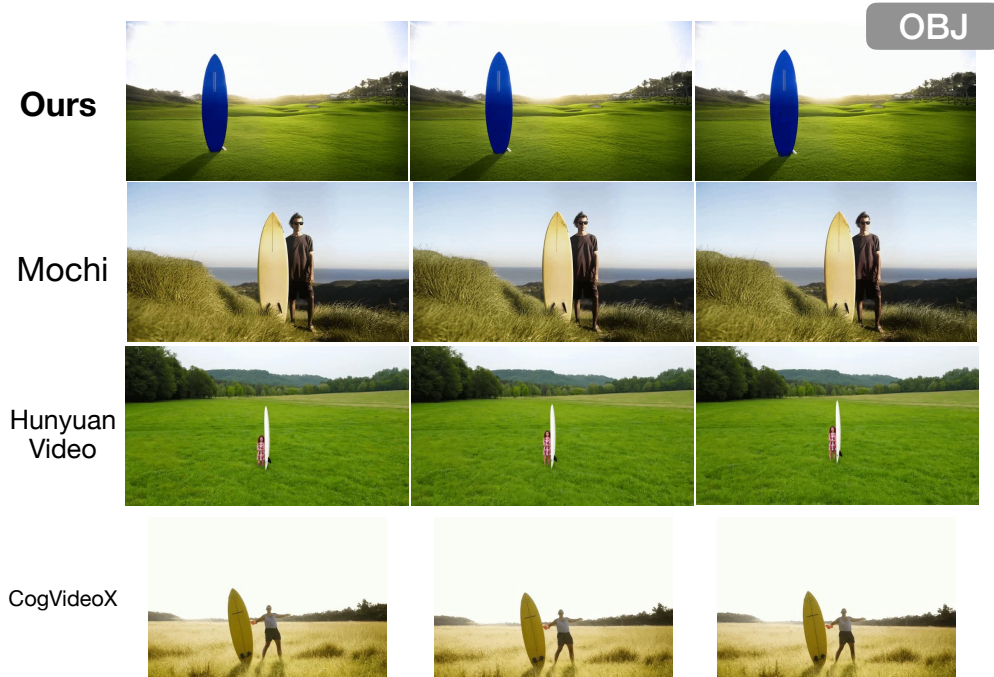
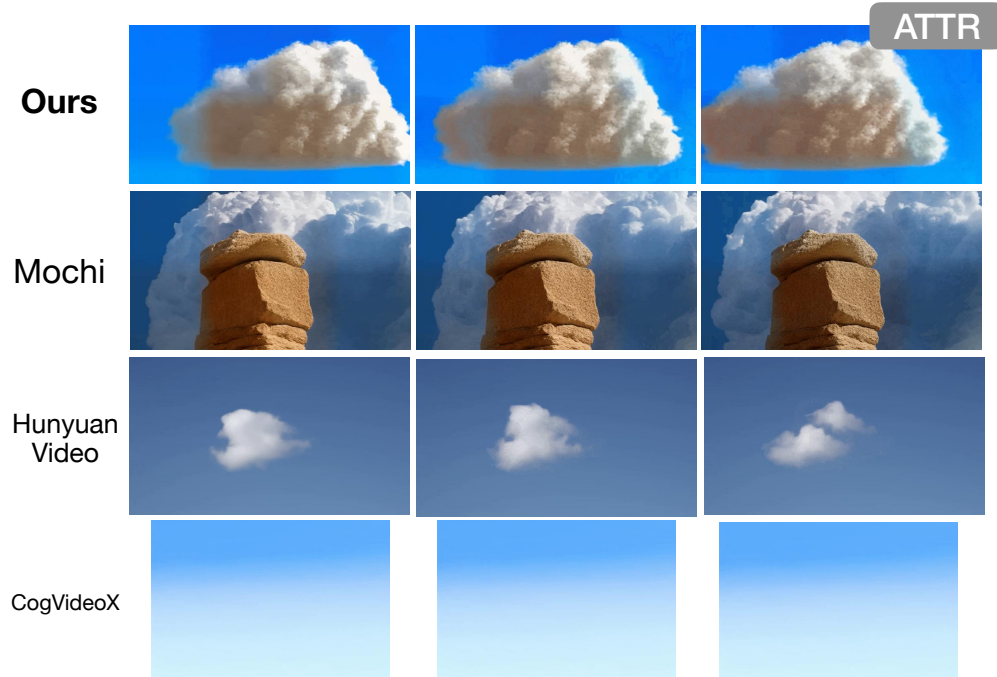


Figure 27: **TEMP.** Prompt: “a sunrise sky with a visible rainbow and moon together.”



*“a surfboard standing in a grassy field”*

Figure 28: **OBJ**. Prompt: “a surfboard standing in a grassy field.”



*“a solid cloud shaped like a rock”*

Figure 29: **ATTR**. Prompt: “a solid cloud shaped like a rock.”



